Geophys. J. Int. (2006) **164,** 633–652 doi: 10.1111/j.1365-246X.2006.02887.x

Dynamic rupture on a planar fault in three-dimensional half space – I. Theory

Haiming Zhang and Xiaofei Chen

Laboratory of Computational Geodynamics, School of Earth & Space Sciences, Peking University, Beijing, 100871, *China. E-mail: xfchen@pku.edu.cn*

Accepted 2005 December 15. Received 2005 November 7; in original form 2005 January 28

SUMMARY

In this study, we extended the boundary integral equation method (BIEM) to include the effect of free surface, which is crucial for the interpretation of near-field observations of large earthquakes on dipping faults, which are buried shallower or rupture to the ground. On the basis of the Green's function in 3-D half space, the boundary integral equations (BIEs) for dynamic rupture propagation on a planar fault embedded in 3-D elastic half space are derived. Since the Green's function can only be expressed as double integration, rather than analytic closed form as in full space, computation of the BIEs for rupture dynamics in half space is rather complicated. Consequently, serious difficulties arise, including the existence of hypersingularities in the kernels and the computation of rapid oscillatory multiple integrals. To resolve them, we first systematically presented the effective regularization procedures, which consists of the generalized Apsel–Luco correction and the regularization algorithm proposed by Karami & Derakhshan to remove the hypersingularities, then proposed a simple while efficient algorithm to speed up the computation of integrals involved in the kernels of BIEs. Finally, the BIEM algorithm proposed in this study for modelling rupture dynamics of a fault with arbitrary dip angle in 3-D half space becomes exercisable, and provides a powerful tool for investigating the physics of earthquake dynamics.

Key words: boundary integral equation, Green's function, half space, planar fault, seismic source dynamics, spontaneous rupture propagation.

1 INTRODUCTION

The geometry of dipping faults, which intersect the free surface, is an important origin of complexities of seismic sources (e.g. Nielsen 1998; Oglesby *et al.* 1998, 2000a,b; Oglesby & Day 2001a,b). Because of strong interaction between the dipping faults and the free surface, large earthquakes, such as the 1999 Chi-Chi, Taiwan, earthquake, usually cause serious damages (Shin & Teng 2001). It is, therefore, of great importance to study the dynamic rupture processes occurring on such faults not only for understanding the physics of seismic sources but also for the efforts in predicting future earthquakes (Oglesby & Day 2001a). However, it is difficult to solve the dynamic rupture processes on dipping faults. On the one hand, spontaneous propagation itself is a highly non-linear moving-boundary problem, which is still a difficult problem in mathematical physics to date; on the other hand, the asymmetric fault geometry makes the problem even more difficult.

To model dynamic rupture of seismic sources, several methods have been applied in the past four decades. Analytic method, first introduced by Kostrov (1966) and then developed by many authors, is of great significance in theoretical analysis. However, since many simplifications must be postulated, it is limited to semi-infinite (Kostrov 1966) or finite (Takeuchi & Kikuchi 1973; Knopoff & Chatterjee 1982; Chatterjee & Knopoff 1983; Chen 1985; Chen *et al.* 1987) 2-D shear crack problems and circular (Kostrov 1964; Burridge & Levy 1974) or elliptic (Burridge & Willis 1969; Richards 1976) 3-D self-similar shear crack problems. To solve a complicated 3-D dynamic rupture problem, one must fall back on numerical methods. Three methods have been widely used for this purpose: the finite-difference method (FDM), the finite-element method (FEM) and the boundary integral equation method (BIEM). The FDM is introduced to dynamic rupture modelling by Madariaga (1976) and Andrews (1976) independently. Since the 1980s, it is developed by many authors (Virieux & Madariaga 1982; Day 1982a,b; Levander 1988; Miyatake 1992; Harris & Day 1993; Mikumo & Miyatake 1995; Madariaga *et al.* 1998; Cruz-Atienza & Virieux 2004), and is now one of the most powerful tools to study rupture propagation. However, the FDM seems to be limited in vertical or horizontal fault geometry owing the regular grid partitioning. Recently, Zhang *et al.* (2004) attempted to break this limit by assuming a 'thick' fault. Unlike the FDM, the FEM is very flexible in treating problems with irregular geometry, and is therefore very popular in many fields of science and engineering. However, huge computation and limited resolution are the major obstacles for the FEM. Although several

authors, such as Archuleta & Frazier (1978) and Archuleta & Day (1980), applied the FEM to model 3-D dynamic problem about 20 yr ago, it is not widely used in dynamic rupture modelling until parallel computing technique is well developed recently (Oglesby *et al.* 1998, 2000a,b; Oglesby & Day 2001a,b; Aagaard 1999; Aagaard *et al.* 2001).

Both the FDM and the FEM belong to the so-called *domain method*, in which the whole domain under consideration must be discretized and solved simultaneously. For a 3-D problem, especially a 3-D infinite-domain problem, a large number of elements must be divided, and therefore the computation is expensive. Besides, the boundary conditions must be treated with great caution. Contrary to the FDM and the FEM, the BIEM falls into the *boundary method*. In this method, only equations on the boundary must be established and solved, and then quantities in the domain can be obtained via integral representation. Compared with the FDM and the FEM, the dimension of the problem to be solved is reduced by one. This merit, as well as the semi-analytic character, makes the BIEM very suitable for solving dynamic rupture problem with stress concentration on the tip of the crack. The BIEM for modelling the dynamic rupture of earthquakes can be divided into two categories, that is, the implicit scheme and the explicit scheme. The implicit BIEM was proposed by Das and her co-workers (Das & Aki 1977; Das 1980, 1981; Das & Kostrov 1987) on the basis of Kostrov's pioneered analytical framework (Kostrov 1966). Although without suffering the hypersingularity difficulty, this method is limited to dynamic rupture problem of a single planar fault embedded in full space. The explicit BIEM, first introduced by Koller *et al.* (1992), not only is easy to incorporate the complex non-linear friction laws, but also can be applied to the problems with complex shaped faults (e.g. curved fault, piecewise planar fault, or step-over faults, etc.). Moreover, it can achieve a superior performance over other methods in both computational efficiency and accuracy after elaborate mathematical treatment on the hypersingualrity of the Green's function. For these reasons, the explicit BIEM is becoming the most favourable tool for studying the dynamic rupture processes of complex earthquake fault systems (e.g. Cochard & Madariaga 1994; Fukuyama & Madariaga 1995, 1998; Chen & Aki 1996; Tada *et al.* 2000; Aochi *et al.* 2000a,b; Aochi & Fukuyama 2002).

However, the medium models used in current studies based on the BIEM have been restricted to elastic full space, because the BIEM depends heavily on the Green's function, and only the Green's function for full space has closed analytic form, which is crucial for establishing the exercisable algorithm of BIEM (see, e.g. Fukuyama & Madariaga 1995, 1998; Tada *et al.* 2000). Full-space model is a good approximation for cases in which the faults are buried at some depth; however, it is invalid when the ruptures run directly to the free surface because of the strong interaction between the fault and the free surface (see, e.g. Nielsen 1998). Although Quin (1990) and Aochi & Fukuyama (2002) attempted to approximately simulate the effect of free surface by introducing imaginary sources for strike-slip faulting, they did not show how to handle the problem for a dipping fault. As a matter of fact, the properness and applicability of so-called *image method* are very limited, because the 3-D elastic waves due to a planar free surface cannot rigorously be represented by any kind of imaginary sources. In reality, ruptures of most disaster earthquakes run onto the ground, or run up to very shallow sediment layer; consequently, the free surface effect cannot be ignored in modelling the dynamic faulting of real earthquakes. Moreover, most of seismic faults are orientated with some dip angle. Therefore, there is an urgent need to develop an accurate and efficient algorithm for modelling the dynamic faulting process of real earthquakes.

In the present study, we shall extend the explicit BIEM to model the dynamic rupture of a dipping fault with an arbitrary dip angle embedded in 3-D elastic half space. The key point of such extension is the using of Green's function for 3-D elastic half space. Although the importance of using half-space Green's function is obvious, there are many difficulties in dealing with such problem. Unlike the full-space case, the Green's function for 3-D elastic half space cannot be expressed in a simple analytical closed form; it is instead represented by double integrations (e.g. Kennett 1983; Chen 1999). Another major obstacle in this extension is the hypersingularity appeared in the boundary integral equations. In this article, we shall systematically present the theoretical development and the detailed methodology of tackling those mathematical difficulties. In the companion article, we shall present the validations of our new method, and the investigations on effects of free surface and faulting obliquity on dynamic rupture processes of earthquakes.

2 FUNDAMENTAL BOUNDARY INTEGRAL EQUATIONS AND THEIR DISCRETIZATION

In this study, we consider the dynamic rupture propagation on a rectangular planar fault, whose length is parallel to the free surface, embedded in an elastic half space, as illustrated in Fig. 1. The fault plane and the free surface are indicated in dark and light gray, respectively. L, W and δ ($0^\circ \leq \delta \leq 90^\circ$) are the length, the width and the dip angle, respectively. $Ox_1x_2x_3$ and $O'x'_1x'_2x'_3$ are coordinate systems built on the free surface and the fault, where axes x_1 and x_2 are in the free surface, and axes x'_1 and x'_2 are in the fault plane. Origins O and O' are concurrent, and axes x_1 and x'_1 are concurrent, which are in consistent with the intersection line of the fault and the free surface. The upper bound of the fault is parallel to the free surface, and the vertical distance between the two is h ($h \geq 0$).

Throughout this study, we suppose only shear slip occurs, that is, the slip is in the fault plane (Mode II and III). Slip is allowed only in the direction of the stress drop, which is assumed to be parallel to x'_1 or x'_2 axis, as usually did in dynamic rupture models (e.g. Fukuyama & Madariaga 1998; Madariaga *et al.* 1998; Aochi *et al.* 2000a,b; Aagaard *et al.* 2001; Aochi & Fukuyama 2002). In other words, two special cases are considered in the present study: dip slip and strike slip. Since the focus of this study is not on nucleation of rupture, we shall initiate the rupture at $t = 0$ by given an artificial 'kick' (see, e.g. Fukuyama & Madariaga 1998; Madariaga *et al.* 1998). This is performed by assuming a small patch (i.e. asperity, Kanamori & Stewart 1978), in which the initial stress is slightly higher than the yield stress.

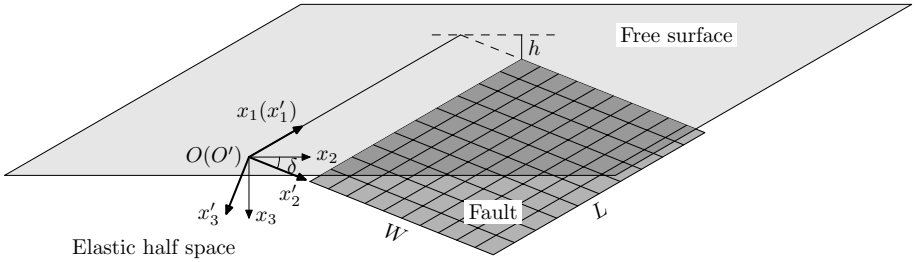

Figure 1. Geometry model of this study. The fault is simplified as a dipping rectangular with length L, width W and a dip angle δ ($0^\circ \le \delta \le 90^\circ$). $h \ge 0$ is the distance between the upper bound of the fault and the free surface. $Ox_1x_2x_3$ and $O'x_1'x_2'x_3'$ are coordinate systems built on the free surface and the fault, where axes x_1 and x_2 are in the free surface, and axes x_1' and x_2' are in the fault plane. Origins O and O' are concurrent, and axes x_1 and x_1' are concurrent, which are in consistent with the intersection line of the fault and the free surface.

2.1 Fundamental boundary integral equations

The start point of the explicit BIEM is the representation theorem (see, e.g. Aki & Richards 1980). In frequency domain, the representation theorem for a fault plane can be written as

$$\tilde{u}_n(\boldsymbol{x}, \omega) = \int\!\!\int_{\Sigma} \Delta\tilde{u}_i(\boldsymbol{\xi}, \omega) c_{ijpq} \nu_j \tilde{G}_{np,q}(\boldsymbol{x}, \boldsymbol{\xi}, \omega)\, dS(\boldsymbol{\xi}), \tag{1}$$

where $\boldsymbol{x}$ and $\boldsymbol{\xi}$ are, respectively, the field and source points, Σ is a fault plane that consist of two opposite surfaces Σ^+ and Σ^-, ω is the circular frequency, $\Delta\tilde{u}_i = \tilde{u}_i|_{\Sigma^+} - \tilde{u}_i|_{\Sigma^-}$ is the slip on the fault, $\tilde{G}_{np}$ is the Green's function for half space, c_{ijpq} and ν_j are the elastic constants and the unit vector normal to the fault. It is noted that $\tilde{(\cdot)}$ denotes quantity in frequency domain. Partial derivatives with respect to x_i and ξ_i are marked as $\partial_i(\cdot)$ and $(\cdot)_{,i}$, respectively. Throughout this paper, Roman subscripts are supposed to run over 1, 2 and 3, while Greek subscripts run over 1 and 2, and Einstein's summation convention over repeated indices is assumed. Quantities in coordinate systems $Ox_1x_2x_3$ and $O'x_1'x_2'x_3'$ are hereafter marked as $(\cdot)$ and $(\cdot)'$, respectively. Occasionally, the same symbol represents different quantities in different context, for example, k denotes the horizontal wavenumber in some context while serving as a subscript/superscript elsewhere, and δ stands for both the dip angle of the fault and the name of Dirac delta function, but we believe no confusion will arise because the meaning of the symbol can be clearly recognized from the context.

To obtain the explicit BIEs, we take the derivative of $\tilde{u}_n$ with respect to x_i

$$\partial_m\tilde{u}_n(\boldsymbol{x}, \omega) = \int\!\!\int_{\Sigma} \Delta\tilde{u}_i(\boldsymbol{\xi}, \omega) c_{ijpq} \nu_j \partial_m \tilde{G}_{np,q}(\boldsymbol{x}, \boldsymbol{\xi}, \omega)\, dS(\boldsymbol{\xi}). \tag{2}$$

Notice that the left-hand side of eq. (2) is the spatial derivative of the unknown $\tilde{u}_n$, and the right-hand side is the sum of weighted integrals of slip $\Delta\tilde{u}_n$, which is also an unknown. It means that the derivatives of displacement on an arbitrary point *in* a half space V can be expressed as the weighted integrals of slip on the fault plane, see Fig. 2(a).

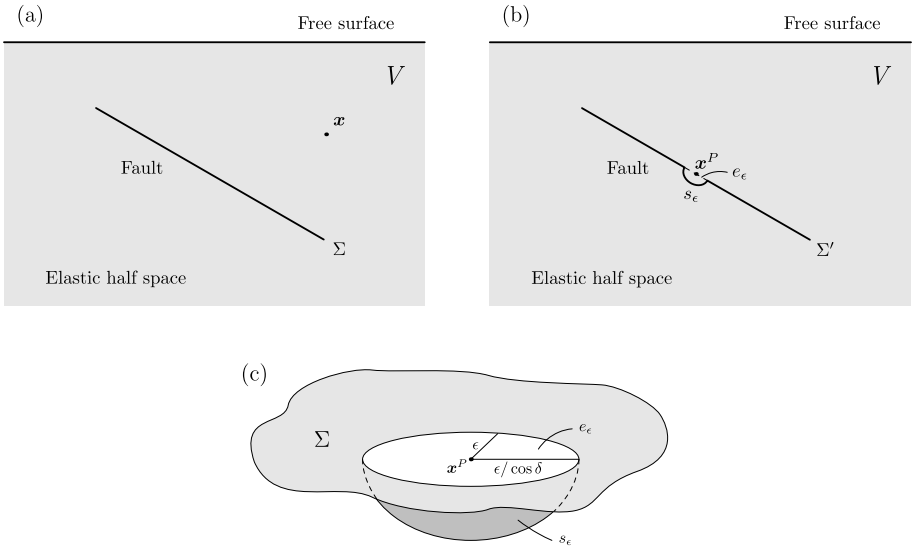

Figure 2. Sketch for changing a boundary point to an inner point. (a) Elastic half space with an inner planar fault Σ. $\boldsymbol{x}$ is an inner point of volume V. (b) Elastic half space with an inner fault Σ', which is composed of the original planar plane without a neighborhood of the original boundary point $\boldsymbol{x}^P$, $\Sigma - e_\epsilon$ and a half rotary ellipsoid s_ϵ. The original boundary point $\boldsymbol{x}^P$ now becomes an inner point. (c) Zoomed figure of neighborhood of $\boldsymbol{x}^P$ in 3-D. The region in white color is an ellipse e_ϵ with half major axis $\epsilon/\cos\delta$ and half minor axis ϵ.

Since for a given point $\boldsymbol{x}$ in the region V, as illustrated in Fig. 2(a), the displacement can be expressed as a surface integral on slip on the fault Σ, the slip $\Delta\tilde{u}_n$ must be calculated first. It is natureal to put $\boldsymbol{x}$ directly on the boundary. However, since eq. (2) is valid only for $\boldsymbol{x}$ *in* the region, we apply the usual manner in BIEM study (e.g. Guiggiani & Gigante 1990; Guiggiani *et al.* 1992; Karami & Derakhshan 1999; Frangi & Guiggiani 2001) to establish the BIEs on boundary.

Let the inner point $\boldsymbol{x}^P$ locate on the fault Σ. We define a new fault plane $\Sigma' = \Sigma - e_\epsilon + s_\epsilon$ (Fig. 2b), in which Σ is the original fault plane, e_ϵ is a small ellipse with $\boldsymbol{x}^P$ on the center, s_ϵ is a half rotary ellipsoid, as illustrated in Fig. 2(c). The half major axis and half minor axis of e_ϵ are $\epsilon/\cos\delta$ and ϵ with $\epsilon \to 0$, such that the projection of e_ϵ onto the Ox_1x_2 plane is a circle with a radius ϵ. Since $\epsilon \to 0$, the surface integral on Σ' tends to that on Σ. In such case as shown in Fig. 2(c), however, the boundary point $\boldsymbol{x}^P$ on original fault Σ now becomes an inner point of region V with Σ'. Therefore, let $\boldsymbol{x} = \boldsymbol{x}^P$, eq. (2) gives

$$\partial_m\tilde{u}_n(\boldsymbol{x}^P,\omega) = \lim_{\epsilon\to 0}\iint_{\Sigma-e_\epsilon} \Delta\tilde{u}_i(\boldsymbol{\xi},\omega) Z_{nim}(\boldsymbol{x}^P,\boldsymbol{\xi},\omega)\,dS(\boldsymbol{\xi}) + \lim_{\epsilon\to 0}\iint_{s_\epsilon} \Delta\tilde{u}_i(\boldsymbol{\xi},\omega) Z_{nim}(\boldsymbol{x}^P,\boldsymbol{\xi},\omega)\,dS(\boldsymbol{\xi}), \tag{3}$$

with $Z_{nim}(\boldsymbol{x}^P,\boldsymbol{\xi},\omega) = c_{ijpq}\nu_j\partial_m\tilde{G}_{np,q}(\boldsymbol{x}^P,\boldsymbol{\xi},\omega)$. Substituting the Taylor's expansion of $\Delta\tilde{u}_i(\boldsymbol{\xi},\omega)$ on s_ϵ

$$\Delta\tilde{u}_i(\boldsymbol{\xi},\omega) = \Delta\tilde{u}_i(\boldsymbol{x}^P,\omega) + \Delta\tilde{u}_{i,k}(\boldsymbol{x}^P,\omega)\left(\xi_k - x_k^P\right) + O(\epsilon^2), \quad \text{for } \boldsymbol{\xi} \text{ on } s_\epsilon \tag{4}$$

into eq. (3) yields

$$\partial_m\tilde{u}_n(\boldsymbol{x}^P,\omega) = \lim_{\epsilon\to 0}\iint_{\Sigma-e_\epsilon} \Delta\tilde{u}_i(\boldsymbol{\xi},\omega) Z_{nim}(\boldsymbol{x}^P,\boldsymbol{\xi},\omega)\,dS(\boldsymbol{\xi}) + \mathcal{I}_1(\boldsymbol{x}^P,\omega) + \mathcal{I}_2(\boldsymbol{x}^P,\omega) + \mathcal{I}_3(\boldsymbol{x}^P,\omega), \tag{5}$$

where

$$\mathcal{I}_1(\boldsymbol{x}^P,\omega) = \lim_{\epsilon\to 0}\iint_{s_\epsilon} O(\epsilon^2) Z_{nim}(\boldsymbol{x}^P,\boldsymbol{\xi},\omega)\,dS(\boldsymbol{\xi}),$$

$$\mathcal{I}_2(\boldsymbol{x}^P,\omega) = \Delta\tilde{u}_i(\boldsymbol{x}^P,\omega)\lim_{\epsilon\to 0}\iint_{s_\epsilon} Z_{nim}(\boldsymbol{x}^P,\boldsymbol{\xi},\omega)\,dS(\boldsymbol{\xi}),$$

$$\mathcal{I}_3(\boldsymbol{x}^P,\omega) = \Delta\tilde{u}_{i,k}(\boldsymbol{x}^P,\omega)\lim_{\epsilon\to 0}\iint_{s_\epsilon}\left(\xi_k - x_k^P\right) Z_{nim}(\boldsymbol{x}^P,\boldsymbol{\xi},\omega)\,dS(\boldsymbol{\xi}).$$

Since the Green's function has weak singularity, that is, $\tilde{G}_{np}(\boldsymbol{x}^P,\boldsymbol{\xi},\omega) \sim O(\frac{1}{\epsilon})$ as $\epsilon \to 0$, $Z_{nim}(\boldsymbol{x}^{P\pm},\boldsymbol{\xi},\omega)$ and $1/\epsilon^3$ are infinities with the same order. $dS \sim \epsilon^2$, thus

$$\mathcal{I}_1(\boldsymbol{x}^P,\omega) = \lim_{\epsilon\to 0} O\left(\epsilon^2\cdot\epsilon^2\cdot\frac{1}{\epsilon^3}\right) = 0, \tag{6}$$

Notice that

$$\lim_{\epsilon\to 0}\iint_{s_\epsilon} Z_{nim}(\boldsymbol{x}^P,\boldsymbol{\xi},\omega)\,dS(\boldsymbol{\xi}) = \lim_{\epsilon\to 0} O\left(\frac{1}{\epsilon}\right),$$

we have

$$\mathcal{I}_2(\boldsymbol{x}^P,\omega) = \lim_{\epsilon\to 0}\frac{\mathcal{A}_{nm}}{\epsilon}, \tag{7}$$

where $\mathcal{A}_{nm}$ is some bounded quantity. Define

$$C_{ikmm} \triangleq \lim_{\epsilon\to 0}\iint_{s_\epsilon}\left(\xi_k - x_k^P\right) Z_{nim}(\boldsymbol{x}^P,\boldsymbol{\xi},\omega)\,dS(\boldsymbol{\xi}),$$

where C_{ikmm} are the so-called *free terms*. Since free terms are bounded terms, many efforts have been made to calculate them in the BIEM studies (e.g. Guiggiani & Gigante 1990; Guiggiani *et al.* 1992; Guiggiani 1995; Mantic & Paris 1996; Young 1996; Frangi & Guiggiani 2001). It is difficult to calculate free terms. Fortunately, however, when a simple box-like discretization scheme is applied (Section 2.2), this difficulty can be avoided. In the present discretization scheme, $\Delta\tilde{u}_{i,k}(\boldsymbol{x}^P,\omega) = 0$, therefore

$$\mathcal{I}_3(\boldsymbol{x}^P,\omega) = 0. \tag{8}$$

With eqs (6)–(8), we obtain

$$\partial_m\tilde{u}_n(\boldsymbol{x}^P,\omega) = \lim_{\epsilon\to 0}\iint_{\Sigma-e_\epsilon} \Delta\tilde{u}_i(\boldsymbol{\xi},\omega) Z_{nim}(\boldsymbol{x}^P,\boldsymbol{\xi},\omega)\,dS(\boldsymbol{\xi}) + \lim_{\epsilon\to 0}\frac{\mathcal{A}_{nm}}{\epsilon}. \tag{9}$$

The stress–tensor field on the fault can be found as follows:

$$\tilde{\tau}_{kl}(\boldsymbol{x}^P,\omega) = c_{klnm}c_{ijpg}\nu_j I_{inp}^{m,q}(\boldsymbol{x}^P,\omega) + \lim_{\epsilon\to 0}\frac{\mathcal{A}'_{kl}}{\epsilon}, \tag{10}$$

and

$$I_{inp}^{m,q}(\boldsymbol{x}^P,\omega) = \lim_{\epsilon\to 0}\iint_{\Sigma-e_\epsilon}\Delta\tilde{u}_i(\boldsymbol{\xi},\omega)\partial_m\tilde{G}_{np,q}(\boldsymbol{x},\boldsymbol{\xi},\omega)\,dS(\boldsymbol{\xi}).$$

The Green's function is solved in coordinate system $Ox_1x_2x_3$ (see Section 3); therefore, it is convenient to calculate the surface integration in $Ox_1x_2x_3$, and then calculate the rupture process on coordinate system $Ox'_1x'_2x'_3$. Project the fault plane $\Sigma - e_\epsilon$ on to the free surface, integral $I^{m,q}_{inp}$ can be expressed as

$$I^{m,q}_{inp}(\boldsymbol{x}^P, \omega) = w_0 \lim_{\epsilon\to 0} \int\!\!\int_{\Sigma'-e'_\epsilon} \left\{\Delta\tilde{u}_i(\boldsymbol{\xi}, \omega)\partial_m \tilde{G}_{np,q}(\boldsymbol{x}^P, \boldsymbol{\xi}, \omega)\right\}_{\xi_3=p_\alpha\xi_\alpha} d\xi_1\, d\xi_2, \tag{11}$$

in which $\Sigma' - e'_\epsilon$ is the projection of $\Sigma - e_\epsilon$ on surface Ox_1x_2, and e'_ϵ is a circle with a radius ϵ. $w_0 = \sqrt{1 + p_1^2 + p_2^2}$, in which p_α is the coefficient of the plane equation of the fault $x_3 = p_\alpha x_\alpha$. For the specific case shown in Fig. 1, $p_1 = 0$ and $p_2 = \tan\delta$. It is noticed that the twice differentiations on the Green's function in eq. (11) results in singularities in the order of $1/\epsilon^3$, that is, the hypersingularities, which are generally non-removable. However, some of them can be regularized by simply integrating by parts (e.g. Sládek & Sládek 1984; Nishimura & Kobayashi 1989; Fukuyama & Madariaga 1995, 1998; Tada *et al.* 2000); the rest remain non-removable that are keys for processing the *regularization* later in the Section 4 aiming at accurately evaluating the value of singular sum in eq. (10). As a matter of fact, the hypersingularities asscociated with derivatives to ξ_1 or ξ_2 can be removed by using the following relations

$$\tilde{G}_{ij,\alpha} = \frac{d}{d\xi_\alpha}\tilde{G}_{ij} - p_\alpha \tilde{G}_{ij,3}, \qquad \partial_\alpha \tilde{G}_{ij} = -\tilde{G}_{ij,\alpha},$$

and taking integration by parts. Finally, the integrals defined in eq. (11) are reduced to the followings:

$$I^{\alpha,\beta}_{inp}(\boldsymbol{x}^P, \omega) = \mathcal{U}_{i\alpha np\beta}(\boldsymbol{x}^P, \omega) - p_\alpha \mathcal{U}_{i\beta np3}(\boldsymbol{x}^P, \omega) - p_\alpha p_\beta \mathcal{W}^{\mathrm{I}}_{inp}(\boldsymbol{x}^P, \omega), \tag{12.1}$$

$$I^{\alpha,3}_{inp}(\boldsymbol{x}^P, \omega) = \mathcal{U}_{i\alpha np\beta}(\boldsymbol{x}^P, \omega) + p_\alpha \mathcal{W}^{\mathrm{I}}_{inp}(\boldsymbol{x}^P, \omega), \tag{12.2}$$

$$I^{3,\beta}_{inp}(\boldsymbol{x}^P, \omega) = -\mathcal{V}_{i\beta np}(\boldsymbol{x}^P, \omega) - p_\beta \mathcal{W}^{\mathrm{II}}_{inp}(\boldsymbol{x}^P, \omega), \tag{12.3}$$

$$I^{3,3}_{inp}(\boldsymbol{x}^P, \omega) = \mathcal{W}^{\mathrm{II}}_{inp}(\boldsymbol{x}^P, \omega), \tag{12.4}$$

in which,

$$\mathcal{U}_{i\alpha npq}(\boldsymbol{x}^P, \omega) = w_0 \lim_{\epsilon\to 0} \int\!\!\int_{\Sigma'-e'_\epsilon} \left\{[\Delta\tilde{u}_{\alpha,1}(\boldsymbol{\xi}, \omega) + p_\alpha \Delta\tilde{u}_{i,3}(\boldsymbol{\xi}, \omega)]\tilde{G}_{np,q}(\boldsymbol{x}^P, \boldsymbol{\xi}, \omega)\right\}_{\xi_3=p_\beta\xi_\beta} d\xi_1\, d\xi_2, \tag{13.1}$$

$$\mathcal{V}_{i\alpha np}(\boldsymbol{x}^P, \omega) = w_0 \lim_{\epsilon\to 0} \int\!\!\int_{\Sigma'-e'_\epsilon} \left\{[\Delta\tilde{u}_{\alpha,1}(\boldsymbol{\xi}, \omega) + p_\alpha \Delta\tilde{u}_{i,3}(\boldsymbol{\xi}, \omega)]\partial_3\tilde{G}_{np}(\boldsymbol{x}^P, \boldsymbol{\xi}, \omega)\right\}_{\xi_3=p_\beta\xi_\beta} d\xi_1\, d\xi_2, \tag{13.2}$$

$$\mathcal{W}^{\mathrm{I}}_{inpj}(\boldsymbol{x}^P, \omega) = w_0 \lim_{\epsilon\to 0} \int\!\!\int_{\Sigma'-e'_\epsilon} \left\{\Delta\tilde{u}_i(\boldsymbol{\xi}, \omega)\tilde{G}_{np,33}(\boldsymbol{x}^P, \boldsymbol{\xi}, \omega)\right\}_{\xi_3=p_\beta\xi_\beta} d\xi_1\, d\xi_2, \tag{13.3}$$

$$\mathcal{W}^{\mathrm{II}}_{inp}(\boldsymbol{x}^P, \omega) = w_0 \lim_{\epsilon\to 0} \int\!\!\int_{\Sigma'-e'_\epsilon} \left\{\Delta\tilde{u}_i(\boldsymbol{\xi}, \omega)\partial_3\tilde{G}_{np,3}(\boldsymbol{x}^P, \boldsymbol{\xi}, \omega)\right\}_{\xi_3=p_\beta\xi_\beta} d\xi_1\, d\xi_2. \tag{13.4}$$

Substituting eqs (12) and (10) into eq. (10), the stress can be written as

$$\begin{aligned}\tilde{\tau}_{kl}(\boldsymbol{x}^P, \omega) = {} & c_{klm\alpha}\nu_j\big\{c_{ijpq}\mathcal{U}_{i\alpha npq}(\boldsymbol{x}^P, \omega) + p_\alpha c_{ijp3}\mathcal{W}^{\mathrm{I}}_{inp}(\boldsymbol{x}^P, \omega) - p_\alpha c_{ijp\beta}\big[\mathcal{U}_{i\beta np3}(\boldsymbol{x}^P, \omega) \\ & + p_\beta \mathcal{W}^{\mathrm{I}}_{inp}(\boldsymbol{x}^P, \omega)\big]\big\} + c_{kln3}\nu_j\big\{c_{ijp3}\mathcal{W}^{\mathrm{II}}_{inp}(\boldsymbol{x}^P, \omega) - c_{ijp\beta}\big[\mathcal{V}_{i\beta np}(\boldsymbol{x}^P, \omega) \\ & + p_\beta \mathcal{W}^{\mathrm{II}}_{inp}(\boldsymbol{x}^P, \omega)\big]\big\} + \lim_{\epsilon\to 0}\frac{\mathcal{A}'_{kl}}{\epsilon}.\end{aligned} \tag{14}$$

And through coordinate transform of tensor, stress in the coordinate system $O'x'_1x'_2x'_3$ can be obtained

$$\tilde{\tau}'_{mn}(\boldsymbol{x}^P, \omega) = M_{m'k}M_{n'l}\tilde{\tau}_{kl}(\boldsymbol{x}^P, \omega), \tag{15}$$

where, $M_{m'k}$ is the coefficient of coordinate transform, and for problem illustrated in Fig. 1,

$$\begin{pmatrix} M_{1'1} & M_{1'2} & M_{1'3} \\ M_{2'1} & M_{2'2} & M_{2'3} \\ M_{3'1} & M_{3'2} & M_{3'3} \end{pmatrix} = \begin{pmatrix} 1 & 0 & 0 \\ 0 & \cos\delta & \sin\delta \\ 0 & -\sin\delta & \cos\delta \end{pmatrix}.$$

So far, the general BIEs, which are independent of specific forms of the Green's function, have been established. It should be pointed out that when the dip angle of the planar fault δ tends to 90° (e.g. $\delta > 60°$), it is convenient to project fault plane onto the Ox_1x_3 plane, rather than the Ox_1x_2 plane, to ensure a proper or stable numerical computation. Derivation of the corresponding BIEs is similar to that above, and is not repeated here for concision.

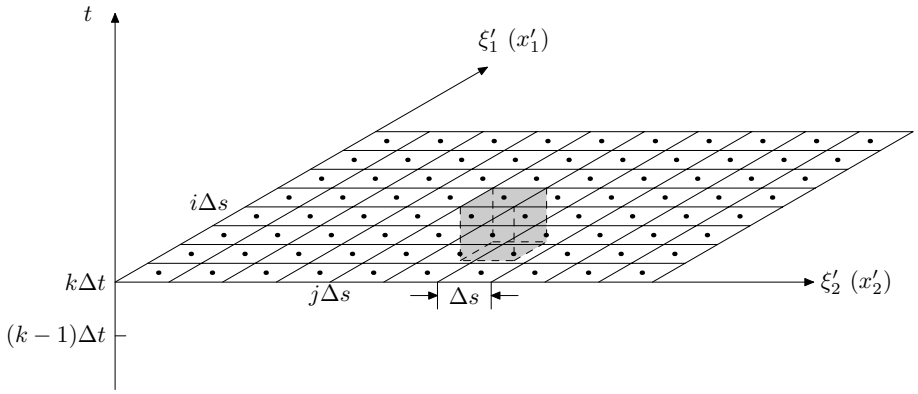

Figure 3. Sketch for discretization scheme. The horizontal plane is the fault plane, vertical axis is time. Dots in center of the cells on the fault plane denote the positions of field point $\boldsymbol{x}^P$. Δs is the space step. Slip rate in the box in grey is constant.

2.2 Discretization of the boundary integral equations

To obtain the forms propitious to numerical computation, a proper discretization scheme must be introduced. Here we adopt a simple box-like discretization scheme (e.g. Cochard & Madariaga 1994; Fukuyama & Madariaga 1998; Aochi *et al.* 2000a)

$$\Delta \dot{u}'_\alpha(\boldsymbol{\xi}', \tau) = \sum_{l,m,n} V_\alpha^{\prime lmn}\left[H\left(\xi_1' - \xi_1^{\prime l}\right) - H\left(\xi_1' - \xi_1^{\prime (l+1)}\right)\right] \cdot\left[H\left(\xi_2' - \xi_2^{\prime m}\right) - H\left(\xi_2' - \xi_2^{\prime (m+1)}\right)\right]\dot{S}(\tau;\tau^n), \qquad (l,\ m = 0, 1, 2, \cdots), \tag{16}$$

where

$$\dot{S}(\tau;\tau^n) = H(\tau - \tau^{n-1}) - H(\tau - \tau^n) \tag{17}$$

and $\tau^n = n\Delta t$. $H(\cdot)$ is the Heaviside function. $\dot{(\cdot)}$ means the partial derivative with respect to time variable t. $V_\alpha^{\prime lmn}$ is the slip rate in a particular element (l, m, n) to be solved. Throughout this paper, (l, m) and n denote the serial numbers of spatial and temporal grids of source point, respectively, while (i, j) and k are those of field points. For example, $(i + \frac{1}{2},\ j + \frac{1}{2},\ k)$ stands for the field point with coordinate $(i\Delta s + \frac{1}{2}\Delta s,\ j\Delta s + \frac{1}{2}\Delta s)$ in coordinate system $O'x_1'x_2'x_3'$ at the instant $k\Delta t$, in which Δs and Δt are spatial and temporal step sizes, respectively. Fig. 3 shows a sketch for the discretization scheme. The horizontal plane is the fault plane, which has been divided into elements with the center points denoting field points. The vertical axis is time axis. According to eq. (16), for fault plane at the instant $k\Delta t$, the slip rate in the cube in gray color in Fig. 3 is constant. For an arbitrary field point, we called the element into which it falls a *collocation element*, and all the other elements *non-collocation elements*.

Substituting eq. (16) into eq. (10) and applying coordinate transform and discretization for field points, we get

$$\mathcal{U}_{s\alpha rpq}^{ij}(\omega) = w_0 M_{\zeta' s} \sum_{l,m,n} V_\zeta^{\prime lmn} \mathcal{D}_{\alpha rpq}^{ij;lm}(\omega)\tilde{S}^n(\omega), \tag{18.1}$$

$$\mathcal{V}_{s\alpha rp}^{ij}(\omega) = w_0 M_{\zeta' s} \sum_{l,m,n} V_\zeta^{\prime lmn} \mathcal{E}_{\alpha rp}^{ij;lm}(\omega)\tilde{S}^n(\omega), \tag{18.2}$$

$$\mathcal{W}_{srp}^{\alpha;ij}(\omega) = w_0 M_{\zeta' s} \sum_{l,m,n} V_\zeta^{\prime lmn} \mathcal{F}_{rp}^{\alpha;ij;lm}(\omega)\tilde{S}^n(\omega), \tag{18.3}$$

with

$$\mathcal{D}_{\alpha rpq}^{ij;lm}(\omega) = \sum_\eta (M_{\eta'\alpha} + p_\alpha M_{\eta' 3}) \lim_{\epsilon\to 0} \iint_{\Sigma' - e'_\epsilon} N_\eta^{lm}(\xi_1, \xi_2)\tilde{G}_{rp,q}^{ij}(\xi_1, \xi_2, \omega)\, d\xi_1\, d\xi_2, \tag{19.1}$$

$$\mathcal{E}_{\alpha rp}^{ij;lm}(\omega) = \sum_\eta (M_{\eta'\alpha} + p_\alpha M_{\eta' 3}) \lim_{\epsilon\to 0} \iint_{\Sigma' - e'_\epsilon} N_\eta^{lm}(\xi_1, \xi_2)\partial_3\tilde{G}_{rp}^{ij}(\xi_1, \xi_2, \omega)\, d\xi_1\, d\xi_2, \tag{19.2}$$

$$\mathcal{F}_{rp}^{\mathrm{I}:ij;lm}(\omega) = \lim_{\epsilon\to 0} \iint_{\Sigma' - e'_\epsilon} N_3^{lm}(\xi_1, \xi_2)\tilde{G}_{rp,33}^{ij}(\xi_1, \xi_2, \omega)\, d\xi_1\, d\xi_2, \tag{19.3}$$

$$\mathcal{F}_{rp}^{\mathrm{II}:ij;lm}(\omega) = \lim_{\epsilon\to 0} \iint_{\Sigma' - e'_\epsilon} N_3^{lm}(\xi_1, \xi_2)\partial_3\tilde{G}_{rp,3}^{ij}(\xi_1, \xi_2, \omega)\, d\xi_1\, d\xi_2, \tag{19.4}$$

and

$$N_1^{lm}(\xi_1,\xi_2) = \left[\delta\left(D_{1\alpha}\xi_\alpha - D_{1\alpha}\zeta_\alpha^{lm}\right) - \delta\left(D_{1\alpha}\xi_\alpha - D_{1\alpha}\zeta_\alpha^{(l+1)(m+1)}\right)\right] \cdot\left[H\left(D_{2\alpha}\xi_\alpha - D_{2\alpha}\zeta_\alpha^{lm}\right) - H\left(D_{2\alpha}\xi_\alpha - D_{2\alpha}\zeta_\alpha^{(l+1)(m+1)}\right)\right],$$

$$N_2^{lm}(\xi_1,\xi_2) = \left[H\left(D_{1\alpha}\xi_\alpha - D_{1\alpha}\zeta_\alpha^{lm}\right) - H\left(D_{1\alpha}\xi_\alpha - D_{1\alpha}\zeta_\alpha^{(l+1)(m+1)}\right)\right] \cdot\left[\delta\left(D_{2\alpha}\xi_\alpha - D_{2\alpha}\zeta_\alpha^{lm}\right) - \delta\left(D_{2\alpha}\xi_\alpha - D_{2\alpha}\zeta_\alpha^{(l+1)(m+1)}\right)\right],$$

$$N_3^{lm}(\xi_1,\xi_2) = \left[H\left(D_{1\alpha}\xi_\alpha - D_{1\alpha}\zeta_\alpha^{lm}\right) - H\left(D_{1\alpha}\xi_\alpha - D_{1\alpha}\zeta_\alpha^{(l+1)(m+1)}\right)\right] \cdot\left[H\left(D_{2\alpha}\xi_\alpha - D_{2\alpha}\zeta_\alpha^{lm}\right) - H\left(D_{2\alpha}\xi_\alpha - D_{2\alpha}\zeta_\alpha^{(l+1)(m+1)}\right)\right],$$

$$\tilde{G}_{rp}^{ij}(\xi_1,\xi_2,\omega) = \tilde{G}_{rp}\left(x_1^{i+\frac{1}{2}}, x_2^{j+\frac{1}{2}}, p_1x_1^{i+\frac{1}{2}} + p_2x_2^{j+\frac{1}{2}}, \xi_1, \xi_2, p_1\xi_1 + p_2\xi_2, \omega\right),$$

$$\tilde{S}^n(\omega) = \frac{1}{\omega^2}(1 - e^{i\omega\Delta t})e^{-i\omega n\Delta t},$$

where

$$D_{\beta\alpha} = M_{\beta'\alpha} + M_{\beta'3}p_\alpha, \qquad \zeta_\alpha^{lm} = (2-\alpha)\xi_1'^{l} + (\alpha-1)\xi_2'^{m},$$

and $\delta(\cdot)$ is the Delta function.

With eqs (14), (18) and (19), we can obtain the discrete BIEs on fault plane according to eq. (15)

$$\tau_{st}'^{ijk} = \sum_{l,m,n} \mathcal{C}_{st\zeta}^{ijk;lmn} V_\zeta'^{lmn}, \tag{20}$$

where

$$\mathcal{C}_{st\zeta}^{ijk;lmn} = \mathcal{F}^{-1}\Big\{M_{s'a}M_{t'b}M_{\zeta'g}\nu_e\Big[c_{abd\alpha}\Big(c_{gepq}\mathcal{D}_{\alpha dpq}^{ij;lm}(\omega) + p_\alpha c_{gep3}\mathcal{F}_{dp}^{\mathrm{I}:ij;lm}(\omega) - p_\alpha c_{gep\beta}\Big(\mathcal{D}_{\beta dp3}^{ij;lm}(\omega) + p_\beta\mathcal{F}_{dp}^{\mathrm{I}:ij;lm}(\omega)\Big)\Big) + c_{abd3}\Big(c_{gep3}\mathcal{F}_{dp}^{\mathrm{II}:ij;lm}(\omega) - c_{gep\beta}\Big(\mathcal{E}_{\beta dp}^{ij;lm}(\omega) + p_\beta\mathcal{F}_{dp}^{\mathrm{I}:ij;lm}(\omega)\Big)\Big)\Big]\cdot\tilde{S}^n(\omega)\Big\}_{t=k\Delta t} + \lim_{\epsilon\to 0}\frac{\mathcal{A}_{st\zeta}^{ijk;lmn}}{\epsilon}, \tag{21}$$

$\mathcal{F}^{-1}(\cdot)$ stands for inverse Fourier transform, and $\mathcal{A}_{st\zeta}^{ijk;lmn}$ is some bounded quantity. We call $\mathcal{C}_{st\zeta}^{ijk;lmn}$ the *kernel* of the BIEs. Notice that eq. (20) is the same as that of Aochi *et al.* (2000a) in form, but the kernels are completely different. On the one hand, the kernels are defined by singular eq. (21), in which there are not only explicit singular terms with order of $1/\epsilon$ (the last term), but also hypersingular terms in the sum within bracket $\{\cdots\}$. Detailed investigation reveals that the collocation elements of $\mathcal{F}_{rp}^{\mathrm{I}:ij;lm}$ and $\mathcal{F}_{rp}^{\mathrm{II}:ij;lm}$ contain the singular terms with order of $1/\epsilon$. On the other hand, kernels $\mathcal{C}_{st\zeta}^{ijk;lmn}$ are physically well-behaved normal quantities, accordingly, their values should be finite, or bounded. Therefore, the parts associated with hypersingularities in the sum within bracket $\{\cdots\}$ must be cancelled by the last explicit infinite term. This will be explored in detail in Section 4.

3 GREEN'S FUNCTION FOR ELASTIC HALF SPACE

In the previous section, we have established the BIEs, which are independent of the special form of Green's function. To calculate dynamic rupture on planar fault in half space, the Green's function for half space in specific forms is required. This is the subject of the present section.

3.1 Green's function for half space

Since the pioneering work of Lamb (1904), numerous authors have studied the Green's functions for different media (e.g. Cagniard 1939; Pekeris 1955a,b; Helmberger 1968; Fuchs & Müller 1971; Johnson 1974; Luco & Apsel 1983; Yao & Harkrider 1983; Chen 1999). The methods can be roughly divided into two categories, the Cagniard–de Hoop method based on Laplace transform, and the wavenumber integration method based on Fourier–Bessel transform. Although solutions in time domain can be directly obtained by Caginard–de Hoop method (Johnson 1974), the spatial derivative of the Green's function involves two-order temporal derivatives, which is inconvenient to numerical computation. In this study, we adopt the Green's function given by the wavenumber integration method. According to Chen's (1999) derivation, the Green's function for half space in frequency domain can be expressed as

$$\tilde{G}_{11}(\boldsymbol{x},\boldsymbol{\xi},\omega) = \frac{1}{4\pi\mu}\left\{\gamma_1^2\left[I_1^{(0)} + I_2^{(0)}\right] + \gamma_2^2\left[I_3^{(0)} + I_4^{(0)}\right]\right\}, \tag{22.1}$$

$$\tilde{G}_{12}(\boldsymbol{x},\boldsymbol{\xi},\omega) = \tilde{G}_{21}(\boldsymbol{x},\boldsymbol{\xi},\omega) = \frac{1}{4\pi\mu}\gamma_1\gamma_2\left\{I_1^{(0)} + I_2^{(0)} - I_3^{(0)} - I_4^{(0)}\right\}, \tag{22.2}$$

$$\tilde{G}_{13}(\boldsymbol{x},\boldsymbol{\xi},\omega) = -\frac{1}{4\pi\mu}\gamma_1 I_5^{(0)}, \tag{22.3}$$

$$\tilde{G}_{22}(\boldsymbol{x},\boldsymbol{\xi},\omega) = \frac{1}{4\pi\mu}\left\{\gamma_2^2\left[I_1^{(0)} + I_2^{(0)}\right] + \gamma_1^2\left[I_3^{(0)} + I_4^{(0)}\right]\right\}, \tag{22.4}$$

$$\tilde{G}_{23}(\boldsymbol{x},\boldsymbol{\xi},\omega) = -\frac{1}{4\pi\mu}\gamma_2 I_5^{(0)}, \tag{22.5}$$

$$\tilde{G}_{31}(\boldsymbol{x},\boldsymbol{\xi},\omega) = -\frac{1}{4\pi\mu}\gamma_1 I_6^{(0)}, \tag{22.6}$$

$$\tilde{G}_{32}(\boldsymbol{x},\boldsymbol{\xi},\omega) = -\frac{1}{4\pi\mu}\gamma_2 I_6^{(0)}, \tag{22.7}$$

$$\tilde{G}_{33}(\boldsymbol{x},\boldsymbol{\xi},\omega) = -\frac{1}{4\pi\mu} I_7^{(0)}, \tag{22.8}$$

where $\gamma_1 = (x_1 - \xi_1)/r$ and $\gamma_2 = (x_2 - \xi_2)/r$ are direction factors,

$$\begin{Bmatrix} I_1^{(0)} \\ I_3^{(0)} \end{Bmatrix} = \frac{1}{2}\int_0^{+\infty} A_{S1}^{(1)}(x_3,\xi_3,k,\omega)\big[J_0(kr) \mp J_2(kr)\big]\frac{1}{k}\,dk, \tag{23.1}$$

$$\begin{Bmatrix} I_2^{(0)} \\ I_4^{(0)} \end{Bmatrix} = \frac{1}{2}\int_0^{+\infty} A_{T}^{(1)}(x_3,\xi_3,k,\omega)\big[J_0(kr) \pm J_2(kr)\big]\frac{1}{k}\,dk, \tag{23.2}$$

$$I_5^{(0)} = \int_0^{+\infty} A_{S0}^{(1)}(x_3,\xi_3,k,\omega)J_1(kr)\frac{1}{k}\,dk, \tag{23.3}$$

$$I_6^{(0)} = \int_0^{+\infty} A_{R1}^{(1)}(x_3,\xi_3,k,\omega)J_1(kr)\frac{1}{k}\,dk, \tag{23.4}$$

$$I_7^{(0)} = \int_0^{+\infty} A_{R0}^{(1)}(x_3,\xi_3,k,\omega)J_0(kr)\frac{1}{k}\,dk, \tag{23.5}$$

and

$$A_{S1}^{(1)}(x_3,\xi_3,k,\omega) = \frac{k^2\beta^2}{\omega^2}\left\{\left(\frac{k^2}{\gamma}e^{\mathrm{P}} - \nu e^{\mathrm{S}}\right) - \frac{\bar{\mathcal{R}}(k)}{\mathcal{R}(k)}\left(\frac{k^2}{\gamma}e^{\mathrm{PP}} + \nu e^{\mathrm{SS}}\right) + \frac{4k^2\nu\chi}{\mathcal{R}(k)}(e^{\mathrm{SP}} + e^{\mathrm{PS}})\right\}, \tag{24.1}$$

$$A_{S0}^{(1)}(x_3,\xi_3,k,\omega) = \frac{k^3\beta^2}{\omega^2}\left\{\mathrm{sgn}(x_3-\xi_3)(e^{\mathrm{P}} - e^{\mathrm{S}}) + \frac{\bar{\mathcal{R}}(k)}{\mathcal{R}(k)}(e^{\mathrm{PP}} + e^{\mathrm{SS}}) - \frac{4\chi}{\mathcal{R}(k)}(k^2 e^{\mathrm{SP}} + \nu\gamma e^{\mathrm{PS}})\right\}, \tag{24.2}$$

$$A_{R1}^{(1)}(x_3,\xi_3,k,\omega) = \frac{k^3\beta^2}{\omega^2}\left\{\mathrm{sgn}(x_3-\xi_3)(e^{\mathrm{P}} - e^{\mathrm{S}}) - \frac{\bar{\mathcal{R}}(k)}{\mathcal{R}(k)}(e^{\mathrm{PP}} + e^{\mathrm{SS}}) + \frac{4\chi}{\mathcal{R}(k)}(\nu\gamma e^{\mathrm{SP}} + k^2 e^{\mathrm{PS}})\right\}, \tag{24.3}$$

$$A_{R0}^{(1)}(x_3,\xi_3,k,\omega) = \frac{k^2\beta^2}{\omega^2}\left\{\left(\gamma e^{\mathrm{P}} - \frac{k^2}{\nu}e^{\mathrm{S}}\right) + \frac{\bar{\mathcal{R}}(k)}{\mathcal{R}(k)}\left(\gamma e^{\mathrm{PP}} + \frac{k^2}{\nu}e^{\mathrm{SS}}\right) - \frac{4k^2\gamma\chi}{\mathcal{R}(k)}(e^{\mathrm{SP}} + e^{\mathrm{PS}})\right\}, \tag{24.4}$$

$$A_{T}^{(1)}(x_3,\xi_3,k,\omega) = \frac{k^2}{\nu}(e^{\mathrm{S}} + e^{\mathrm{SS}}), \tag{24.5}$$

with

$$e^{\mathrm{P}} = e^{-\gamma|x_3-\xi_3|}, \quad e^{\mathrm{S}} = e^{-\nu|x_3-\xi_3|}, \quad e^{\mathrm{PP}} = e^{-\gamma(x_3+\xi_3)}, \quad e^{\mathrm{SS}} = e^{-\nu(x_3+\xi_3)},$$

$$e^{\mathrm{SP}} = e^{-(\gamma x_3+\nu\xi_3)}, \quad e^{\mathrm{PS}} = e^{-(\gamma\xi_3+\nu x_3)},$$

$\gamma = \sqrt{k^2-(\omega/\alpha)^2}$ $(Re(\gamma) > 0)$, $\nu = \sqrt{k^2-(\omega/\beta)^2}$ $(Re(\nu) > 0)$, $\chi = 2k^2 - (\omega/\beta)^2$, $\mathcal{R}(k) = \chi^2 - 4k^2\nu\gamma$ is the Rayleigh function $\bar{\mathcal{R}}(k) = \chi^2 + 4k^2\nu\gamma$, α and β are the P and S velocity, respectively, k is the horizontal wavenumber, ω is the circular frequency, $r = \sqrt{(x_1-\xi_1)^2 + (x_2-\xi_2)^2}$, $\mathrm{sgn}(\cdot)$ is the sign function and $J_m(x)$ is the m-th order Bessel function.

It is worth noticing that in $\omega - k$ domain, the contributions from the free surface are separated from those of direct waves. It can be proved in mathematics that if the terms corresponding to the contributions from the free surface are removed, the Green's function above is exactly the same as those for full space.

3.2 Spatial derivatives of the Green's function

The following terms must be solved before returning to the discrete BIEs in eq. (20)

$$\tilde{G}_{ij,k}, \quad \partial_3\tilde{G}_{ij}, \quad \tilde{G}_{ij,33}, \quad \partial_3\tilde{G}_{ij,3}. \quad (i,j,k = 1,2,3)$$

We can see from eqs (22)–(24) that the terms involving x_3 and ξ_3 are separated from those involving other spatial coordinates, and x_3 and ξ_3 appear only in the powers of exponential terms. Therefore, it is very convenient to calculate the derivatives with respect to x_3 or/and ξ_3

(Appendix A). However, it is rather more complicated to calculate $\tilde{G}_{ij,\alpha}$, because both the Bessel functions and the direction factors γ_1 and γ_2 are functions of ξ_1 and ξ_2. Notice that

$$r_{,\alpha} = -\gamma_\alpha, \qquad \gamma_{\beta,\alpha} = \frac{\gamma_\alpha\gamma_\beta - \delta_{\alpha\beta}}{r},$$

and

$$J_0(kr) - J_2(kr) = 2J_1'(kr), \quad J_0(kr) + J_2(kr) = \frac{2}{kr}J_1(kr), \quad J_1''(kr) = \frac{1}{kr}J_2(kr) - J_1(kr).$$

$\tilde{G}_{ij,\alpha}$ can be obtained as

$$\tilde{G}_{11,1}(\boldsymbol{x},\boldsymbol{\xi},\omega) = \frac{\gamma_1}{4\pi\mu}\left\{\frac{2\left(\gamma_1^2-1\right)}{r}\left[I_1^{(0)}+I_2^{(0)}\right] + \frac{2\gamma_2^2}{r}\left[I_3^{(0)}+I_4^{(0)}\right] - \gamma_1^2\left[I_1^{(1)}+I_2^{(1)}\right] - \gamma_2^2\left[I_3^{(1)}+I_4^{(1)}\right]\right\}, \tag{25.1}$$

$$\tilde{G}_{12,1}(\boldsymbol{x},\boldsymbol{\xi},\omega) = \tilde{G}_{21,1}(\boldsymbol{x},\boldsymbol{\xi},\omega) = \frac{\gamma_2}{4\pi\mu}\left\{\frac{2\gamma_1^2-1}{r}\left[I_1^{(0)}+I_2^{(0)}-I_3^{(0)}-I_4^{(0)}\right] - \gamma_1^2\left[I_1^{(1)}+I_2^{(1)}-I_3^{(1)}-I_4^{(1)}\right]\right\}, \tag{25.2}$$

$$\tilde{G}_{13,1}(\boldsymbol{x},\boldsymbol{\xi},\omega) = \frac{1}{4\pi\mu}\left\{\frac{1-\gamma_1^2}{r}I_5^{(0)} + \gamma_1^2 I_5^{(1)}\right\}, \tag{25.3}$$

$$\tilde{G}_{22,1}(\boldsymbol{x},\boldsymbol{\xi},\omega) = \frac{\gamma_1}{4\pi\mu}\left\{\frac{2\left(\gamma_1^2-1\right)}{r}\left[I_3^{(0)}+I_4^{(0)}\right] + \frac{2\gamma_2^2}{r}\left[I_1^{(0)}+I_2^{(0)}\right] - \gamma_1^2\left[I_3^{(1)}+I_4^{(1)}\right] - \gamma_2^2\left[I_1^{(1)}+I_2^{(1)}\right]\right\}, \tag{25.4}$$

$$\tilde{G}_{23,1}(\boldsymbol{x},\boldsymbol{\xi},\omega) = -\frac{\gamma_1\gamma_2}{4\pi\mu}\left\{\frac{1}{r}I_5^{(0)} - I_5^{(1)}\right\}, \tag{25.5}$$

$$\tilde{G}_{31,1}(\boldsymbol{x},\boldsymbol{\xi},\omega) = \frac{1}{4\pi\mu}\left\{\frac{1-\gamma_1^2}{r}I_6^{(0)} + \gamma_1^2 I_6^{(1)}\right\}, \tag{25.6}$$

$$\tilde{G}_{32,1}(\boldsymbol{x},\boldsymbol{\xi},\omega) = -\frac{\gamma_1\gamma_2}{4\pi\mu}\left\{\frac{1}{r}I_6^{(0)} - I_6^{(1)}\right\}, \tag{25.7}$$

$$\tilde{G}_{33,1}(\boldsymbol{x},\boldsymbol{\xi},\omega) = \frac{\gamma_1}{4\pi\mu}I_7^{(1)}, \tag{25.8}$$

$$\tilde{G}_{11,2}(\boldsymbol{x},\boldsymbol{\xi},\omega) = \frac{\gamma_2}{4\pi\mu}\left\{\frac{2\left(\gamma_2^2-1\right)}{r}\left[I_3^{(0)}+I_4^{(0)}\right] + \frac{2\gamma_1^2}{r}\left[I_1^{(0)}+I_2^{(0)}\right] - \gamma_1^2\left[I_1^{(1)}+I_2^{(1)}\right] - \gamma_2^2\left[I_3^{(1)}+I_4^{(1)}\right]\right\}, \tag{25.9}$$

$$\tilde{G}_{12,2}(\boldsymbol{x},\boldsymbol{\xi},\omega) = \tilde{G}_{21,1}(\boldsymbol{x},\boldsymbol{\xi},\omega) = \frac{\gamma_1}{4\pi\mu}\left\{\frac{\gamma_2^2-1}{r}\left[I_1^{(0)}+I_2^{(0)}-I_3^{(0)}-I_4^{(0)}\right] - \gamma_2^2\left[I_1^{(1)}+I_2^{(1)}-I_3^{(1)}-I_4^{(1)}\right]\right\}, \tag{25.10}$$

$$\tilde{G}_{13,2}(\boldsymbol{x},\boldsymbol{\xi},\omega) = \tilde{G}_{23,1}(\boldsymbol{x},\boldsymbol{\xi},\omega), \tag{25.11}$$

$$\tilde{G}_{22,2}(\boldsymbol{x},\boldsymbol{\xi},\omega) = \frac{\gamma_2}{4\pi\mu}\left\{\frac{2\left(\gamma_2^2-1\right)}{r}\left[I_1^{(0)}+I_2^{(0)}\right] + \frac{2\gamma_1^2}{r}\left[I_3^{(0)}+I_4^{(0)}\right] - \gamma_1^2\left[I_3^{(1)}+I_4^{(1)}\right] - \gamma_2^2\left[I_1^{(1)}+I_2^{(1)}\right]\right\}, \tag{25.12}$$

$$\tilde{G}_{23,2}(\boldsymbol{x},\boldsymbol{\xi},\omega) = \frac{1}{4\pi\mu}\left\{\frac{1-\gamma_2^2}{r}I_5^{(0)} + \gamma_2^2 I_5^{(1)}\right\}, \tag{25.13}$$

$$\tilde{G}_{31,2}(\boldsymbol{x},\boldsymbol{\xi},\omega) = \tilde{G}_{32,1}(\boldsymbol{x},\boldsymbol{\xi},\omega), \tag{25.14}$$

$$\tilde{G}_{32,2}(\boldsymbol{x},\boldsymbol{\xi},\omega) = \frac{1}{4\pi\mu}\left\{\frac{1-\gamma_2^2}{r}I_6^{(0)} + \gamma_2^2 I_6^{(1)}\right\}, \tag{25.15}$$

$$\tilde{G}_{33,2}(\boldsymbol{x},\boldsymbol{\xi},\omega) = \frac{\gamma_2}{4\pi\mu}I_7^{(1)}, \tag{25.16}$$

where

$$\begin{Bmatrix} I_1^{(1)} \\ I_4^{(1)} \end{Bmatrix} = \int_0^{+\infty} \begin{bmatrix} A_{S1}^{(1)} \\ A_T^{(1)} \end{bmatrix} (x_3,\xi_3,k,\omega)\left[\frac{1}{kr}J_2(kr) - J_1(kr)\right] dk, \tag{26.1}$$

$$\begin{Bmatrix} I_2^{(1)} \\ I_3^{(1)} \end{Bmatrix} = -\int_0^{+\infty} \frac{1}{kr} \begin{Bmatrix} A_T^{(1)} \\ A_{S1}^{(1)} \end{Bmatrix} (x_3, \xi_3, k, \omega) J_2(kr)\, dk, \tag{26.2}$$

$$I_5^{(1)} = \int_0^{+\infty} A_{S0}^{(1)}(x_3, \xi_3, k, \omega) J_1'(kr)\, dk, \tag{26.3}$$

$$I_6^{(1)} = \int_0^{+\infty} A_{R1}^{(1)}(x_3, \xi_3, k, \omega) J_1'(kr)\, dk, \tag{26.4}$$

$$I_7^{(1)} = -\int_0^{+\infty} A_{R0}^{(1)}(x_3, \xi_3, k, \omega) J_1(kr)\, dk. \tag{26.5}$$

4 REGULARIZATION OF THE INTEGRAL KERNELS

So far we have obtained the discrete BIEs and the specific Green's function for half space. It is obvious that to calculate the dynamic rupture process, one must calculate the integral kernels by substituting the Green's function into the BIEs that are in singular form as mentioned previously. We shall regularize the singular equations by a regularization procedure. Our regularization procedure consists of two steps: first, efficiently separate the singular parts from the Green's function by taking generalized Apsel-Luco corrections; then, precisely separate the hypersingularities in the BIEs, and impose them to be exactly cancelled out with the explicit singular term.

4.1 Generalized Apsel-Luco corrections

The aim in this part is to separate the singular parts from $I_p^{(q)}$ ($p = 1, 2, \ldots, 7; q = 0, 1, \ldots, 5$) in eqs (23), (26) and (A3). According to eqs (23), (24), (A3)–(A7), the power of k increases with the increase of orders of spatial derivatives with respect to x_3 or ξ_3. This will lead the integrands to be infinity at $k \to +\infty$ when $x_3 \to \xi_3$, which is difficult to compute numerically. If the parts involving powers of k, which can be carried out analytically, are separated from the integrals, such that the remaining parts are transformed to proper integrals, then the problem is solved. Fortunately, this can be realized by applying the Taylor's expansions at $k \to +\infty$ and the integrals involving the Bessel functions.

Take the simplest $I = I_2^{(4)} + I_4^{(4)}$ (see, eq. A3.2) for an example

$$I = I^{\text{full}} + I^{\text{surf}} = \int_0^{+\infty} A_T^{\text{full}(4)}(x_3, \xi_3, k, \omega) J_0(kr)\, dk + \int_0^{+\infty} A_T^{\text{surf}(4)}(x_3, \xi_3, k, \omega) J_0(kr)\, dk, \tag{27}$$

where, $A_T^{\text{full}(4)} = k\nu \exp(-\nu|x_3 - \xi_3|)$ and $A_T^{\text{surf}(4)} = k\nu \exp(-\nu(x_3 + \xi_3))$ are terms due to full space and the free surface, respectively. Notice that I is singular only in the case of $R = |\boldsymbol{x} - \boldsymbol{\xi}| \to 0$, therefore singularity arises only from I^{full}, and I^{surf} is a proper integral amenable to numerical computation. The singular I^{full} can be written as

$$\begin{aligned} I^{\text{full}} = &\int_0^{+\infty} \left[A_T^{\text{full}(4)}(x_3, \xi_3, k, \omega) - A_T^{\text{asy}(4)}(x_3, \xi_3, k, \omega)\right] J_0(kr)\, dk \\ &+ \int_0^{+\infty} A_T^{\text{asy}(4)}(x_3, \xi_3, k, \omega) J_0(kr)\, dk, \end{aligned} \tag{28}$$

where

$$A_T^{\text{asy}(4)}(x_3, \xi_3, k, \omega) = \left[k^2 + \frac{\omega^2}{2\beta^2}|x_3 - \xi_3|\, k - \frac{\omega^2}{2\beta^2} + \frac{\omega^4}{8\beta^4}(x_3 - \xi_3)^2\right] e^{-k|x_3 - \xi_3|} \tag{29}$$

is the Taylor's expansion of $A_T^{\text{full}(4)}$. After subtracting $A_T^{\text{asy}(4)}$, the first integral in eq. (28) becomes a proper integral, and singularity is transformed into the second integral, which has analytic results. It is worth mentioning that although the first integral is proper, the integrand converges slowly as $x_3 \to \xi_3$. The peak and trough averaging method (Zhang *et al.* 2003) can be applied to overcome this difficulty. If we define $Q_{mn}(r, x_3 - \xi_3)$ by

$$Q_{mn}(r, x_3 - \xi_3) = \int_0^{+\infty} e^{-k|x_3 - \xi_3|} J_m(kr) k^n\, dk, \quad (m = 0,\ 1,\ 2;\ n = 0,\ 1,\ 2,\ 3)$$

then the second term in eq. (28) can be expressed as

$$\begin{aligned} \int_0^{+\infty} A_T^{\text{asy}(4)}(x_3, \xi_3, k, \omega) J_0(kr)\, dk = {} & Q_{02}(r, x_3 - \xi_3) + \frac{\omega^2}{2\beta^2}|x_3 - \xi_3|\, Q_{01}(r, x_3 - \xi_3) \\ & - \left[\frac{\omega^2}{2\beta^2} - \frac{\omega^4}{8\beta^4}(x_3 - \xi_3)^2\right] Q_{00}(r, x_3 - \xi_3), \end{aligned} \tag{30}$$

where

$$Q_{00}(r, x_3 - \xi_3) = \frac{1}{R}, \qquad Q_{01}(r, x_3 - \xi_3) = \frac{|x_3 - \xi_3|}{R^3}, \qquad Q_{02}(r, x_3 - \xi_3) = \frac{2(x_3 - \xi_3)^2 - r^2}{R^5}. \tag{31}$$

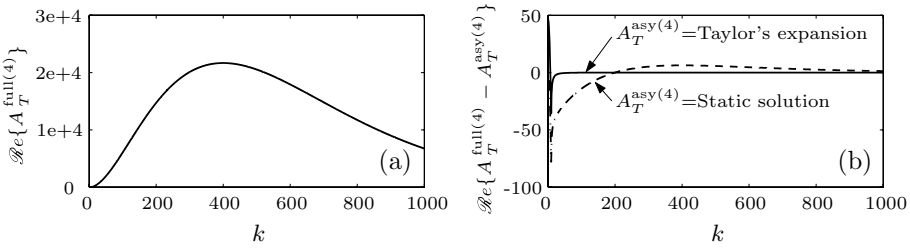

Figure 4. Comparisons of the integrands before and after applying the generalized Aspel-Luco coorection. (a) Real part of $A_T^{\text{full}(4)}$ before correction. (b) Comparison of real parts of $A_T^{\text{full}(4)} - A_T^{\text{asy}(4)}$ after correction with $A_T^{\text{asy}(4)}$ being the Taylor's expansion (solid line) and the static solution (dashed line). $|x_3 - \xi_3| = 0.005$ km, $\omega = 30.4 - 0.5\,\text{i}$ and $\beta = 3.16$ km s^{-1}.

According to the specific expressions of Q_{mn} in eq. (31), the integral in eq. (30) has a singularity up to three order, that is, hypersingularity, as $R \to 0$. The technique described above can be applied to all the integrals $I_p^{(q)}$ ($p = 1, 2, \ldots, 7; q = 0, 1, \ldots, 5$). Complete expressions for all Q_{mn} ($m = 0, 1, 2; n = 0, 1, 2, 3$) needed and the Taylor's expansions $A_{S1}^{\text{asy}(i)}$, $A_{S0}^{\text{asy}(i)}$, $A_{R1}^{\text{asy}(i)}$, $A_{R0}^{\text{asy}(i)}$, $A_T^{\text{asy}(i)}$ ($i = 1, 2, \ldots, 5$) are listed in Appendix B.

Such idea was originally proposed by Apsel & Luco (1983) for efficiently computing Green's function in multilayered media. In their study, the static Green's functions in half space were adopted as asymptotic expressions. Although this can speed up the convergence, it is still very slow due to the difference of models. This technique then was improved by Hisada (1994, 1995) by using static Green's functions for multilayered media as asymptotic expressions. Instead of the *static* Green's functions, we here have taken the Taylor's expansions of Green's functions as asymptotic expressions, and archived better performance. Take the above $A_T^{\text{full}(4)}(x_3, \xi_3, k, \omega)$ for an example. As shown in Fig. 4(a), $A_T^{\text{full}(4)}(x_3, \xi_3, k, \omega)$ converges very slowly to zero with the increase of wavenumber k as $|x_3 - \xi_3| = 0.005$ km. However, $A_T^{\text{full}(4)}(x_3, \xi_3, k, \omega) - A_T^{\text{asy}(4)}(x_3, \xi_3, k, \omega)$ after the generalized Apsel-Luco correction (solid line) converges to zero very quickly (Fig. 4b). For comparison, we also show the result of taking the static solution (dashed line) $A_T^{\text{asy}(4)}(x_3, \xi_3, k, \omega)$ as asymptotic expressions, as Apsel & Luco (1983) did. It is clear that the Taylor's expansion is a better choice. It is interesting that asymptotic expressions, given in eq. (B1), degenerate to static solutions as $\omega \to 0$. For this reason, the technique used here can be regarded as a generalized version of the method of Apsel & Luco (1983), and called the generalized Apsel-Luco correction.

4.2 Separation of hypersingular parts in surface integrals

After the Apsel-Luco correction, singular parts in the wavenumber k integrals of Green's function for half space are separated with an analytical expressions. Consequently, the singular parts of the integrals given in eq. (19) are separated analytically. It is noticed that the *pure* singular terms plus any terms with finite values are still singular. We are facing such situation in singular eq. (21), only the pure singular terms are needed to be exactly cancelled out, and the remained terms are just the kernels we wanted. In what follows we shall describe how to exactly separate, from eq. (19), the *pure* singular terms that are explicitly with the order of $1/\epsilon$ by applying an efficient method proposed by Karami & Derakhshan (1999).

It is noticed that all singularities arise from $\mathcal{F}_{rs}^{\alpha:ij;lm}(\omega)$ in eqs (19.3) and (19.4) for collocation element. Surface integrals involving Q_{mn} for collocation element can be written as

$$P_{pqsmn}^{\text{col}} = \lim_{\epsilon \to 0} \iint_{R^{\text{col}} - e'_\epsilon} \frac{u_1^p \, |u_2|^q}{r^s} Q_{mn}(u_1, u_2)\, du_1 du_2, \tag{32}$$

where $u_1 = x_1 - \xi_1$, $u_2 = x_2 - \xi_2$ and R^{col} denotes the region of $[-\frac{1}{2}\Delta s, \frac{1}{2}\Delta s] \times [-\frac{1}{2}\Delta s \cos\delta, \frac{1}{2}\Delta s \cos\delta]$. In our problem, (p, q, s) runs over (0, 2, 2), (2, 0, 2), (0, 1, 1) and (0, 0, 0). According to eq. (B2), Q_{mn} has an $(n + 1)$-order singularity as $R \to 0$. Therefore, the singularity in eq. (32) has an order of $n + s - p - q + 1 = 1$ (weak singularity) or 3 (hypersingularity).

Rewrite the integral in eq. (32) in local cooridnates ξ_i, then the region under consideration $R^{\text{col}} - e'_\epsilon$ will be transformed into $R^{\text{unit}} - e''_\epsilon$, in which R^{unit} is a rectangular domain of $[-1, 1] \times [-1, 1]$ (Fig. 5). In Fig. 5, the gray region represents the region of integral. e'_ϵ, a circle with radius ϵ, is transformed into an ellipse e''_ϵ.

Let $\xi_1 = \rho \cos\phi$ and $\xi_2 = \rho \sin\phi$, then P_{pqsmn}^{col} can be written in a polar coordinate as

$$P_{pqsmn}^{\text{col}} = \left(\frac{\Delta s}{2}\right)^{p+q+1-s-n} \eta_1^{q+1} \lim_{\epsilon \to 0} \int_0^{2\pi} \left[\int_{\rho_\epsilon(\phi)}^{\rho_M(\phi)} \rho^{p+q-s-n}\, d\rho \right] \frac{\cos^p\phi \, |\sin\phi|^q}{[M(\phi)]^s} Q'_{mn}(\phi)\, d\phi, \tag{33}$$

where $M(\phi) = \sqrt{\cos^2\phi + \eta_1^2 \sin^2\phi}$, $\eta_1 = \cos\delta$, and $\rho_\varepsilon(\phi)$ and $\rho_M(\phi)$ are the upper and lower bound, respectively (Fig. 5b),

$$Q'_{00}(\phi) = 1, \qquad Q'_{01}(\phi) = \eta_2 |\sin\phi|,$$
$$Q'_{02}(\phi) = \left(2\eta_2^2 - \eta_1^2\right)\sin^2\phi - \cos^2\phi, \quad Q'_{03}(\phi) = 3\eta_2 |\sin\phi| \left[\left(2\eta_2^2 - 3\eta_1^2\right)\sin^2\phi - 3\cos^2\phi\right],$$

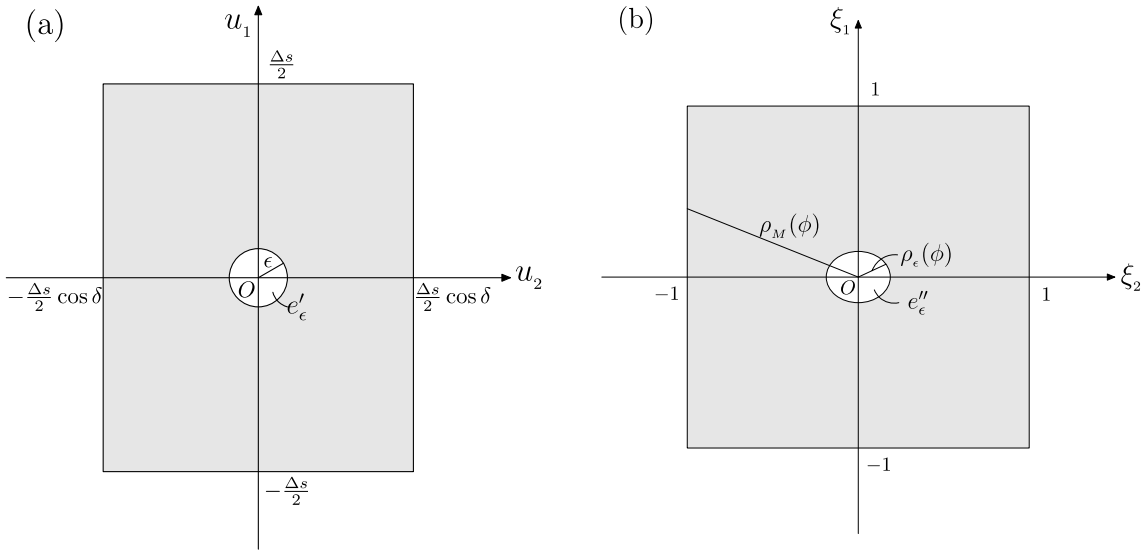

Figure 5. Transformation of the region for collocation element. (a) Projection of Collocation element on the free surface. e'_ϵ is a circle with a radius ϵ ($\epsilon \to 0$). Δs is the space step. δ is the dip angle of the fault. (b) Transformation of the collocation element into a local coordinate. e'_ϵ now becomes an ellipse e''_ϵ, $\rho_\epsilon(\phi)$ is the polar axis of the ellipse and $\rho_M(\phi)$ is the polar ellipse of the boundary of the collocation element.

$$Q'_{10}(\phi) = \frac{1-\eta_2|\sin\phi|}{M(\phi)}, \qquad Q'_{11}(\phi) = M(\phi),$$

$$Q'_{12}(\phi) = 3\eta_2|\sin\phi|M(\phi), \quad Q'_{13}(\phi) = 3M(\phi)\left[\left(4\eta_2^2-\eta_1^2\right)\sin^2\phi - \cos^2\phi\right],$$

$$Q'_{20}(\phi) = [Q'_{10}(\phi)]^2, \qquad Q'_{21}(\phi) = \frac{2Q'_{10}(\phi)}{M(\phi)} - Q'_{01}(\phi),$$

$$Q'_{22}(\phi) = 3[M(\phi)]^2, \qquad Q'_{23}(\phi) = 15\eta_2|\sin\phi|[M(\phi)]^2,$$

with $\eta_2 = \sin\delta$.

For weak singular integrals ($p+q-s-n=0$), the integrals in polar coordinate are transformed into proper integrals naturally. Therefore, according to eq. (33),

$$P^{\rm col}_{pqsmn} = \left(\frac{\Delta s}{2}\right)^{p+q+1-s-n} \frac{\eta_1^{q+1}}{p+q-s-n+1}\int_0^{2\pi}[\rho_M(\phi)]^{p+q-s-n+1}\frac{\cos^p\phi|\sin\phi|^q}{[M(\phi)]^s}Q'_{mn}(\phi)\,d\phi.$$

for $p+q-s-n \geq 0$

While for hypersingular integrals ($p+q-s-n=-2$), the integrals in polar coordinate are still strong ones with factor of $1/\rho^2$. We can obtain from eq. (33) that

$$P^{\rm col}_{pqsmn} = \lim_{\epsilon\to 0}\int_0^{2\pi}\frac{f(\phi)}{\rho_\epsilon(\phi)}\,d\phi - \int_0^{2\pi}\frac{f(\phi)}{\rho_M(\phi)}\,d\phi, \tag{34}$$

where

$$f(\phi) = \left(\frac{2}{\Delta s}\right)\eta_1^{q+1}\frac{\cos^p\phi|\sin\phi|^q}{[M(\phi)]^s}Q'_{mn}(\phi). \tag{35}$$

Substituting $r = \varepsilon = \rho_\varepsilon(\phi)M(\phi)$ (Karami & Derakhshan 1999) into eq. (34) yields

$$P^{\rm col}_{pqsmn} = \lim_{\epsilon\to 0}\frac{1}{\epsilon}\int_0^{2\pi} f(\phi)M(\phi)\,d\phi - \int_0^{2\pi}\frac{f(\phi)}{\rho_M(\phi)}\,d\phi. \tag{36}$$

In eq. (36), the first term with factor $1/\epsilon$ is isolated explicitly, which are imposed to be cancelled out by the last terms with the same order in eq. (21).

5 NUMERICAL TECHNIQUES FOR CALCULATING THE KERNELS

After the above regularization procedures, all the singularities are removed, and the integrals in the kernels are transformed into proper integrals, which can be directly applied to numerical computation in principle. However, these are rapid oscillatory multiple integrals, including a wavenumber k integral and a surface integral. If an ordinary integration scheme is used, it will be too time-consuming and can hardly be applied in practical computation. Therefore, we developed an efficient numerical technique to speed up the computation of these integrals based on detailed analysis on the integrands, and it is summarized as follows.

Since the integrands vary more complicated with wavenumber k than the coordinates on the fault surface ξ_α, it is convenient to change the integration order, that is, to integrate on ξ_α firstly, and then on k. The rapid oscillatory integrals on space variable involved in the kernels are the following two kinds

$$B^{\mathrm{I}}_{pqm}\left(k, u_1, u_2^L, u_2^U, \kappa\right) = \int_{u_2^L}^{u_2^U} \frac{u_2^p}{r^q} e^{-\kappa|u_2|} J_m(kr)\, du_2, \tag{37}$$

$$B^{\mathrm{II}}_{pqnm}\left(k, u_1^L, u_1^U, u_2^L, u_2^U, \kappa\right) = \int_{u_2^L}^{u_2^U}\int_{u_1^L}^{u_1^U} \frac{u_1^p u_2^q}{r^n} e^{-\kappa|u_2|} J_m(kr)\, du_1\, du_2, \tag{38}$$

where $u_1 = x_1 - \xi_1$, $u_2 = x_2 - \xi_2$, $u_1^L = (i - l - \frac{1}{2})\Delta s$, $u_1^U = (i - l + \frac{1}{2})\Delta s$, $u_2^L = (j - m - \frac{1}{2})\Delta s$, $u_2^U = (j - m + \frac{1}{2})\Delta s$, $\kappa = \sqrt{k^2 - \frac{\omega^2}{c^2}}$, with c being the P or S velocity. Notice that κ is a complex as $k < |\frac{\omega}{c}|$, therefore the exponential factor $e^{-\kappa|u_2|}$ is oscillatory with k. Combined with the Bessel function, the integrands become complicated oscillatory functions. It is difficult to calculate the integrals, especially when the imaginary part of κ is large, because according to ordinary integration scheme, the integration step over the whole range must be small enough to ensure a given precision, which is obviously inefficient. We will introduce an efficient integration scheme, which is a combination of self-adaptive sampling based on proximate period estimation and the standard Gaussian integration, to speed up the computation of these multiple integrals. In following, we take B^{I}_{pqm} for an example to describe the algorithm.

Note that the part with non-periodic variation can be neglected when we estimate the proximate period. Let $\kappa = \kappa_{\mathrm{R}} + \mathrm{i}\,\kappa_{\mathrm{I}}$, in which κ_{R}, $\kappa_{\mathrm{I}} \in \mathbb{R}$ are real and imaginary part of κ, respectively. Since the period of Bessel function over whole definition domain is similar to that of asymptotic solution as the argument is large enough,

$$\begin{aligned} f(k, u_1, u_2, \kappa) &= \frac{u_2^p}{r^q} e^{-\kappa|u_2|} J_m(kr) \\ &\sim e^{-\kappa_{\mathrm{R}}|u_2|}[\cos(\kappa_{\mathrm{I}}|u_2|) - \mathrm{i}\,\sin(\kappa_{\mathrm{I}}|u_2|)]\sqrt{\frac{2}{\pi kr}}\cos\left(kr - \frac{m\pi}{2} - \frac{\pi}{4}\right) \\ &\sim \cos\left(|\kappa_{\mathrm{I}} u_2| + k\sqrt{u_1^2 + u_2^2}\right) + \cos\left(\kappa_{\mathrm{I}} u_2| - k\sqrt{u_1^2 + u_2^2}\right), \end{aligned} \tag{39}$$

where '$\sim$' connects two functions with similar periods. It can be seen that the period varies with u_2. Strict instant period should be calculated by Hilbert transformation (e.g. David 1996). Since only the approximate period rather than a strict one is needed, we use a simple algorithm to estimate the period. If the instant period for a given u_2 is marked as $T(u_2)$, then $T(u_2)$ satisfies

$$|\kappa_{\mathrm{I}}|(|u_2| + T(u_2)) + k\sqrt{u_1^2 + (|u_2| + T(u_2))^2} = |\kappa_{\mathrm{I}}| \cdot |u_2| + k\sqrt{u_1^2 + u_2^2} + 2\pi.$$

Solving the above equation, we obtain

$$T(u_2) = \begin{cases} \dfrac{|\kappa_{\mathrm{I}}|A + u_2\left(k^2 - \kappa_{\mathrm{I}}^2\right) - k\sqrt{A^2 + \left(\kappa_{\mathrm{I}}^2 - k^2\right)u_1^2}}{\kappa_{\mathrm{I}}^2 - k^2}, & k \neq |\kappa_{\mathrm{I}}| \\ \dfrac{2\pi(\pi + kr)}{kA}, & k = |\kappa_{\mathrm{I}}| \neq 0 \\ \infty, & k = |\kappa_{\mathrm{I}}| = 0 \end{cases} \tag{40}$$

where we define

$$A = |\kappa_{\mathrm{I}}| \cdot |u_2| + k\sqrt{u_1^2 + u_2^2} + 2\pi.$$

For a given u_2, take the period calculated according to eq. (40) as step size and get the next u_2. A series of subintervals can be obtained in the same way. Then on each subinterval, the variation of integration is gentle enough to apply the standard Gauss integration scheme. Fig. 6(a) shows the division of subintervals for oscillatory $f(k, u_1, u_2, \kappa)$ according to the algorithm based on approximate period estimation described above. $T(u_2)$ calculated by eq. (40) is showed in Fig. 6(b). It can be seen that subinterval division can well describe the variation of the oscillatory integrand. Accordingly, the efficiency of computation can be greatly enhanced.

After the computation of B^{I}_{pqm}, we must continue to compute the integrals on wavenumber k in the form of

$$\int_0^{+\infty} F(k) B^{\mathrm{I}}_{pqm}(k, u_1, u_2^L, u_2^U, \omega)\, dk,$$

in which $F(k)$ is a smooth function of variable k. This is also an oscillatory integral. Although we do not know the exact analytic forms of B^{I}_{pqm}, we can roughly estimate the vibration period. Notice that $F(k)$ does not influence the period of whole integrand, we have

$$\begin{aligned} F(k)B^{\mathrm{I}}_{pqm}(k) &\sim e^{-\sqrt{k^2 - \frac{\omega^2}{c^2}}\,u_2^{\max}} \cos(k\Delta) \\ &\sim \begin{cases} \cos(k\Delta), & k \geq \left|\frac{\omega}{c}\right| \\ \cos\left(k\Delta + u_2^{\max}\sqrt{\frac{\omega^2}{c^2} - k^2}\right) + \cos\left(k\Delta - u_2^{\max}\sqrt{\frac{\omega^2}{c^2} - k^2}\right), & k < \left|\frac{\omega}{c}\right| \end{cases} \end{aligned} \tag{41}$$

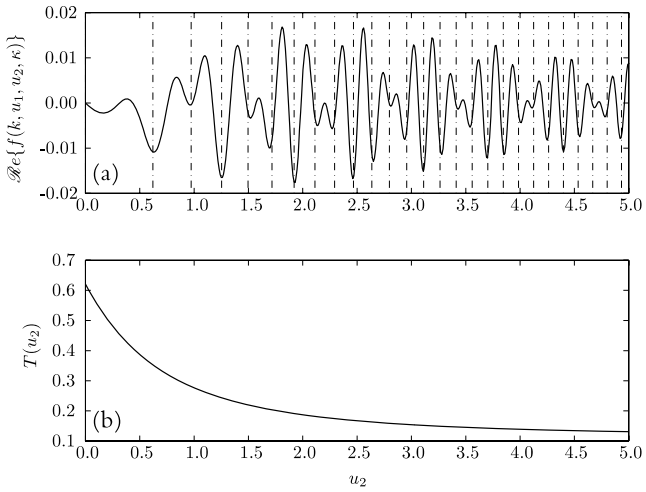

Figure 6. (a) Real part of the oscillatory integrand $f(k, u_1, u_2, \kappa)$ against u_2 (see text, for more details). Vertical dashed lines indicate the subintervals divided on the basis of the approximate period estimation. (b) Approximate period $T(u_2)$ calculated by eq. (40). Parameters for computation are: $k = 50$, $u_1 = 3$, $\kappa = 0.3 + 5$ i, $p = q = m = 1$.

where $u_2^{\max} = \max(|u_2^L|, |u_2^U|)$ and $\Delta = \sqrt{u_1^2 + (u_2^{\max})^2}$. Let $T(k)$ be the instant period at a given k, then $T(k) = \frac{2\pi}{\Delta}$ as $k \geq |\frac{\omega}{c}|$. When $k < |\frac{\omega}{c}|$, since the expression in eq. (41) is similar to that in eq. (39) except that the variable is now k, we can solve $T(k)$ in a similar procedure and obtain

$$T(k) = \frac{P\Delta - kV + u_2^{\max}\sqrt{\frac{\omega^2}{c^2}V - P^2}}{V}, \qquad \text{as} \quad k < \left|\frac{\omega}{c}\right|$$

in which $V = (u_2^{\max})^2 + \Delta^2$, and $P = k\Delta + u_2^{\max}\sqrt{\frac{\omega^2}{c^2} - k^2} + 2\pi$. Once the approximate period is determined, we can apply the scheme described in the preceding paragraph to compute the integrals on k.

Similar algorithm can be applied to B^{II}_{pqnm} and the subsequent computation of integrals on k, which is more complicated. To show the accuracy and efficiency of the above algorithm, Table 1 lists the comparison of results of B^{II}_{pqnm} calculated by the present study and those by MATLAB software. As we know, MATLAB is a powerful tool for numerical computation, therefore we take the results provided by MATLAB as references. The computation parameters are $k = 10.0$, $u_1^L = 1.5$, $u_1^U = 2.5$, $u_2^L = 2.4749$, $u_2^U = 3.1820$, and $\kappa = 0.3318 + 15.0266$ i. Since MATLAB uses an ordinary integration scheme, while the algorithm above is based on detailed analysis on the properties of integrands, the computation time required in the algorithm described above is only about 1 per cent of that in MATLAB for a given precision ($\sim 10^{-6}$). Therefore, the computation of integral kernels of BIEs can be greatly enhanced by the new algorithm.

It is worth mentioning that, although no singularity arises when calculating B^{II}_{pqnm} for non-collocation elements according to eq. (38), a numerical difficulty with the type '$\frac{0}{0}$' will be encountered. To overcome such a difficulty in numerical computation and ensure the stability, the integral is transformed to the following proper form by taking a similar procedure as did in Section 4.2

$$B^{\mathrm{II}}_{pqmn} = \left(\frac{\Delta s}{2}\right)^{p+q+2-n} (\cos\delta)^{q+1} \int_0^{2\pi}\int_0^{\rho_M(\phi)} \rho^{p+q+1-n} \frac{\cos^p\phi\,|\sin\phi|^q}{[M(\phi)]^n} e^{-\kappa\frac{\Delta s}{2}\eta_1\rho|\sin\phi|} \cdot J_m\left(\frac{\Delta s}{2}k\rho M(\phi)\right) d\rho\, d\phi.$$

Table 1. Comparisons of results of B^{II}_{pqnm} calculated by this study and those by MATLAB software. As can be seen, for a give precision 10^{-6}, the CPU time required in this study is much smaller than that in Matlab. For computation, we take the following parameters: $k = 10.0$, $u_1^L = 1.5$, $u_1^U = 2.5$, $u_2^L = 2.4749$, $u_2^{\mathrm{U}} = 3.1820$ and $\kappa = 0.3318 + 15.0266$ i.

	Present study	Matlab
B^{II}_{0000}	$-0.0009483 + 0.0000266$ i	$-0.0009483 + 0.0000266$ i
B^{II}_{0220}	$-0.0007605 + 0.0002138$ i	$-0.0007605 + 0.0002138$ i
B^{II}_{2020}	$-0.0001878 - 0.0001871$ i	$-0.0001878 - 0.0001870$ i
B^{II}_{0111}	$0.0002584 + 0.0011493$ i	$0.0002583 + 0.0011493$ i
B^{II}_{0222}	$0.0007731 - 0.0001433$ i	$0.0007732 - 0.0001433$ i
B^{II}_{2022}	$0.0001837 + 0.0001978$ i	$0.0001837 + 0.0001977$ i
Precision	$\sim 10^{-6}$	10^{-6}
CPU time	$\sim$0.016 s	1.688 s

6 CONCLUSIONS AND DISCUSSIONS

As a first step to the goal of extending the BIEM, which is a powerful tool to study earthquake rupture dynamics on complicated fault systems but limited to full space medium model to date, to a more realistic medium model, we systematically derived the BIEs for modelling earthquake rupture dynamics on a planar fault embedded in half space medium based on the Green's function for half space. Starting from the representation theorem for seismic fault, we derived the BIEs in general form based on elaborate limit analysis. With box-like discretization scheme and the specific forms of Green's function for half space, the corresponding discrete BIEs are obtained. Although they are in the same form as those for modelling rupture dynamics in full space (e.g. Fukuyama & Madariaga 1998; Aochi *et al.* 2000a), the kernels, which are the key factors for dynamic rupture computation, are completely different. Our kernels for half-space problem are given via a singular equation that consists of both explicit and implicit singular terms. Regularization procedures are then applied to exactly extract the implicit singular terms from hypersingular integrals, and finally both explicit and implicit terms are imposed to be cancelled out each other to return physically meaningful bounded kernels in eq. (21). Although the singularities have been removed after regularization, most of the integrals in the kernels are the rapid oscillatory multiple integrals that converge very slowly if an ordinary integration algorithm is taken. Such difficulty is overcome by an effective technique we proposed, and the corresponding computation has been accelerated up to 100 times.

With these techniques, computation time of kernels become acceptable if parallel computation is performed. For example, to compute all the kernels for the dynamic model of a planar fault, which is divided into 80×20 elements, it will take about 4.8 h by using a 16 nodes PC Cluster (each node consists of a single Intel P4 CPU with 2 GHz clock rate and 1 GB RAM). Our BIEM has two important advantages. First, the resolution is higher than pure numerical methods, such as FDM and FEM. For example, in the computation of kernels for very near-field case, the maximum frequency is up to 5 Hz, which is difficult to achieve in FEM and FDM. One example of the maximum frequency in FEM is 0.6 Hz (Oglesby & Day 2001a). Therefore more details of the rupture processes can be revealed by BIEM. Second, in our scheme, the computation of kernels and dynamic rupture process is separated. The former is time-consuming, while the latter is efficient. Fortunately, no physical parameter is required in the computation of kernels. Once the geometry of the fault is known, the kernels can be computed without any knowledge of the physical process of rupture. Therefore, it is possible to build a database in advance for a given fault. Once a database is built, it can be used for dynamic model repeatedly. Therefore, it is obvious that for large amount of dynamic simulation, our scheme is more efficient than FDM and FEM. For example, for an fault divided into 80×20 elements, it will take about 1 h to compute 450 time steps on a single processor PC (with 2 GHz clock rate and 1 GB RAM). If a fast convolution algorithm is applied, the computation time will even remarkably reduced (Aochi *et al.* 2000a).

In summary, the new BIEM for modelling rupture dynamics of fault with an arbitrary dip angle in 3-D half space is exercisable and provides a powerful tool for investigating the physics of earthquake dynamics, though it is still more time-consuming than algorithm for full-space problem (e.g. Fukuyama & Madariaga 1995, 1998; Aochi *et al.* 2000a; Tada *et al.* 2000). The validity and applicability of our new BIEM algorithm will be presented in the companion paper.

ACKNOWLEDGMENTS

This work is supported by National Nature Science Foundation of China (Grant No. 40134010) and National Basic Research Program of China (Grant No. 2004CB418404).

REFERENCES

Aagaard, B.T., 1999. Finite-element simulation of earthquakes, *PhD thesis,* California Institute of Technology, California.

Aagaard, B.T., Heaton, T.H. & Hall, J.F., 2001. Dynamic earthquake ruptures in the presence of lithostatic normal stresses: implications for friction models and heat production, *Bull. seism. Soc. Am.,* **91,** 1765–1796.

Aki, K. & Richards, P.G., 1980. *Quantitative seismology: theory and methods*, W.H. Freeman and Company, San Francisco.

Andrews, D.J., 1976. Rupture propagation with finite stress in antiplane strain, *J. geophys. Res.,* **81,** 3575–3582.

Apsel, R.J. & Luco, J.E., 1983. On the Green's functions for a layered half-space. Part I I, *Bull. seism. Soc. Am.,* **73,** 931–951.

Aochi, H. & Fukuyama, E., 2002. Three-dimensional nonplanar simulation of the 1992 Landers earthquake, *J. geophys. Res.,* **107,** 2035, doi:10.1029/2000JB000061.

Aochi, H., Fukuyama, E. & Matsu'ura, M., 2000a. Spontaneous rupture propagation on a non-planar fault in 3-D elastic medium, *Pure Appl. Geophys.,* **157,** 2003–2027.

Aochi, H., Fukuyama, E. & Matsu'ura, M., 2000b. Selectivity of spontaneous rupture propagation on a branched fault, *Geophys. Res. Lett.,* **27,** 3635–3638.

Archuleta, R.J. & Day, S.M., 1980. Dynamic rupture in a layered medium: the 1966 Parkfield earthquake, *Bull. seism. Soc. Am.,* **70,** 671–689.

Archuleta, R.J. & Frazier, G.A., 1978. Three-dimensional numerical simulations of dynamic faulting in a half-space, *Bull. seism. Soc. Am.,* **68,** 541–572.

Burridge, R. & Levy, C., 1974. Self-similar circular shear cracks lacking cohension, *Bull. seism. Soc. Am.,* **64,** 1789–1808.

Burridge, R. & Willis, J., 1969. The self-similar problem of the expanding elliptical crack in an anisotropic solid, *Proc. Cambridge Phil. Soc.,* **66,** 443–468.

Cagniard, L., 1939. *Réflexion et réfraction des ondes séismiques progressives*, Gauthier-Villars, Paris.

Chatterjee, A.K. & Knopoff, L., 1983. Bilateral propagation of a spontaneous two-dimensional anti-plane shear crack under the influence of cohesion, *Geophys. J. R. astr. Soc.,* **73,** 449–473.

Chen, X.F., 1985. Spontaneous expansion of 2D sesimic fault under the influence of inhomogeneous cohension modulus and friction (in Chinese), *Master Thesis,* Institute of Geophysics, China Earthquake Administration, Beijing.

Chen, X.F., 1999. Seismogram synthesis in multi-layered half-space Part I. Theoretical formulations, *Earth. Res. China,* **13,** 149–174.

Chen, X.F. & Aki, K., 1996. An effective approach to determine the dynamic source parameters, *Pure Appl. Geophys.,* **146,** 689–696.

Chen, Y.T., Chen, X.F. & Knopoff, L., 1987. Spontaneous growth and autonomous contraction of a two-dimensional earthquake fault, *Tectonophysics,* **144,** 5–17.

Cochard, A. & Madariaga, R., 1994. Dynamic faulting under rate-dependent friction. *Pure Appl. Geophys.,* **142,** 419–445.

Cruz-Atienza, V.M. & Virieux, J., 2004. Dynamic rupture simulation of non-planar faults with a finite-defference approach, *Geophys. J. Int.,* **158,** 939–954.

Das, S., 1980. A numerical method for determination of source time functions for general three-dimensional rupture propagation, *Geophy. J. R. astr. Soc.,* **62,** 591–604.

Das, S., 1981. Three-dimensional rupture propagation and implications for the earthquake source mechanism, *Geopys. J. R. astr. Soc.,* **67,** 375–393.

Das, S. & Aki, K., 1977. A numerical study of two-dimensional spontaneous rupture propagation, *Geophy. J. R. astr. Soc.,* **50,** 643–668.

Das, S. & Kostrov, B.V., 1987. On the numerical boundary integral equation method for 3-D shear-crack problems, *J. Appl. Mech.,* **54,** 99–104.

David, V., 1996. On the analytic signal, the Teager-Kaiser energy algorithm, and other methods for defining amplitude and frequecy, *IEEE Trans. Signal Proc.,* **44,** 791–797.

Day, S.M., 1982a. Three-dimensional finite difference simulation of fault dynamics: rectangular faults with fixed rupture velocity, *Bull. seism. Soc. Am.,* **72,** 705–727.

Day, S.M., 1982b. Three-dimensional simulation of spontaneous rupture: the effect of nonuniform prestress, *Bull. seism. Soc. Am.,* **72,** 1881–1902.

Frangi, A. & Guiggiani, M., 2001. Free term and compatibility conditions for 3D hypersingular boundary integral equations, *Z. Angew. Math. Mech.,* **81,** 651–664.

Fuchs, K. & Müller, G., 1971. Computaion of synthetic seismograms with the reflectivity method and comparison of observations, *Geophys. J. R. astr. Soc.,* **23,** 417–433.

Fukuyama, E. & Madariaga, R., 1995. Integral equation method for plane crack with arbitrary shape in 3D elastic medium, *Bull. seism. Soc. Am.,* **85,** 614–628.

Fukuyama, E. & Madariaga, R., 1998. Rupture dynamics of a plannar fault in a 3D elastic medium: rate- and slip-weakening friction, *Bull. seism. Soc. Am.,* **88,** 1–17.

Guiggiani, M., 1995. Hypersingular boundary integral equation have additional free term, *Comput. Mech.,* **16,** 245–248.

Guiggiani, M. & Gigante, A., 1990. A general algorithm for multidimensional Cauchy principal value integrals in the boundary element method, ASME *J. Appl. Mech.,* **57,** 906–915.

Guiggiani, M., Krishnasamy, G., Rudolphi, T. & Rizzo, F.J., 1992. A general algorithm for the numerical solution of hypersingular boundary integral equations, ASME *J. Appl. Mech.,* **59,** 604–614.

Harris, R.A. & Day, S.M., 1993. Dynamics of fault interaction: parallel strike-slip faults, *J. geophys. Res.,* **98,** 4461–4472.

Helmberger, D.V., 1968. The crust-mantle transition in the Bering sea, *Bull. seism. Soc. Am.,* **58,** 179–214.

Hisada, Y., 1994. An efficent method for computing Green's functions for a layered half-space with sources and receivers at close depths, *Bull. seism. Soc. Am.,* **84,** 1456–1472.

Hisada, Y., 1995. An efficent method for computing Green's functions for a layered half-space with sources and receivers at close depths (Part 2), *Bull. seism. Soc. Am.,* **85,** 1080–1093.

Johnson, L., 1974. Green's function for Lamb's problem, *Geophys. J. R. astr. Soc.,* **37,** 99–131.

Kanamori, H. & Stewart, G.S., 1978. Seismological aspects of the Guatemala Earthquake of February 4, 1976, *J. geophys. Res.,* **83,** 3427–3434.

Karami, G. & Derakhshan, D., 1999. An efficient method to evaluate hypersingular and supersingular integrals in boundary integrals equations analysis, *Engng. Anal. Boundary Elements,* **23,** 317–326.

Kennett, B.L.N., 1983. *Seismic wave propagation in stratified media*, Cambridge University Press, New York.

Knopoff, L. & Chatterjee, A., 1982. Unilateral extension of a two-dimensional shear crack under the influence of cohesive forces, *Geophys. J. R. astr. Soc.,* **68,** 7–25.

Koller, M.G., Bonnet, M. & Madariaga, R., 1992. Modelling of dynamical crack propagation using time-domain boundary integral equations, *Wave Motion,* **16,** 339–366.

Kostrov, B.V., 1964. Self-similar problems of propagation of shear cracks, *J. Appl. Math. Mech.,* **28,** 1077–1087.

Kostrov, B.V., 1966. Unsteady propagation of longitudinal shear cracks. *J. Appl. Math. Mech.,* **30,** 1241–1248.

Lamb, H., 1904. On the propagation of tremors over the surface of an elastic solid, *Phil. Trans. R. Soc. London A,* **203,** 1–42.

Levander, A., 1988. Fourth-order finite-difference P-SV seismograms, *Geophysics,* **53,** 1425–1436.

Luco, J.E. & Apsel, R.J., 1983. On the Green's functions for a layered half-space. Part I, *Bull. seism. Soc. Am.,* **73,** 909–929.

Madariaga, R., 1976. Dynamic of an expanding circular fault, *Bull. seism. Soc. Am.,* **66,** 639–667.

Madariaga, R., Olsen, K.B. & Archuleta, R.J., 1998. Modeling dynamic rupture in a 3D earthquake fault model, *Bull. seism. Soc. Am.,* **88,** 1182–1197.

Mantic, V. & Paris, R., 1996. Existence and evaluation of the two free terms in the hypersingular boundary integral equation of potential theory, *Engng. Anal. Boundary Elements,* **16,** 253–260.

Mikumo, T. & Miyatake, T., 1995. Heterogeneous distribution of dynamic stress drop and relative fault strength recovered from the results of waveform inversion, *Bull. seism. Soc. Am.,* **85,** 178–193.

Miyatake, T., 1992. Reconstruction of dynamic rupture process of an earthquake with constrains of kinematic parameters, *Geophys. Res. Lett.,* **19,** 349–352.

Nielsen, S.B., 1998. Free surface effects on the propagation of dynamic rupture, *Geophys. Res. Lett.,* **25,** 125–128.

Nishimura, N. & Kobayashi, S., 1989. A regularized boundary integral equation method for elastodynamic crack problems, *Comput. Mech.,* **4,** 319–328.

Oglesby, D.D., Archuleta, R.J. & Nielsen, S.B., 1998. Earthquakes on dipping faults: the effects of broken symmetry, *Science,* **280,** 1055–1059.

Oglesby, D.D., Archuleta, R.J. & Nielson, S.B., 2000a. The three-dimensional dynamics of dipping faults, *Bull. seism. Soc. Am.,* **90,** 616–628.

Oglesby, D.D., Archuleta, R.J. & Nielson, S.B., 2000b. The dynamics of dipping faulting: explorations in two dimensions, *J. geophys. Res.,* **105,** 13 643–13 653.

Oglesby, D.D. & Day, S.M., 2001a. The effect of fault geometry on the 1999 Chi-Chi (Taiwan) earthquake, *Geophys. Res. Lett.,* **28,** 1831–1834.

Oglesby, D.D. & Day, S.M., 2001b. Fault geometry and the dynamics of the 1999 Chi-Chi (Taiwan) earthquake, *Bull. seism. Soc. Am.,* **91,** 1099–1111.

Pekeris, C., 1955a. The seismic surface pulse, *Proc. Nat. acad. Sci.,* **41,** 469–480.

Pekeris, C., 1955b. The seismic buried pulse, *Proc. Nat. acad. Sci.,* **41,** 629–639.

Quin, H., 1990. Dynamic stress drop and rupture dynamics of the October 15, 1979 Imperial Valley, California, earthquake, *Tectonophysics,* **175,** 93–117.

Richards, P.G., 1976. Dynamic motions near an earthquake fault: a three-dimensional solution, *Bull. seism. Soc. Am.,* **66,** 1–32.

Shin, T.C. & Teng, T.L., 2001. An overview of the 1999 Chi-Chi, Taiwain, earthquake, *Bull. seism. Soc. Am.,* **91,** 895–914.

Sládek, V. & Sládek, J., 1984. Transient elastodynamic three-dimensional problems in crack bodies, *Appl. Math. Modelling,* **8,** 2–10.

Tada, T., Fukuyama, E. & Madariaga, R., 2000. Non-hypersingular boundary integral equations for 3-D non-planar crack dynamics. *Comput. Mech.,* **25,** 613–626.

Takeuchi, H. & Kikuchi, M., 1973. A dynamic model of crack propagation, *J. Phys. Earth,* **21,** 27–37.

Virieux, J. & Madariaga, R., 1982. Dynamic faulting studied by a finite difference method, *Bull. seism. Soc. Am.,* **72,** 345–369.

Yao, Z.X. & Harkrider, D.G., 1983. A generalized reflection-transmission coefficent matrix and discrete wavenumber method for synthetic seismograms, *Bull. seism. Soc. Am.,* **73,** 1685–1699.

Young, A., 1996. A single-domain boundary element method for 3-D elastostatic crack analysis using continuous elements, *Int. J. Num. Meth. Engng.,* **39,** 1265–1293.

Zhang, H.M., Chen, X.F. & Chang, S.H., 2003. An efficient method for computing synthetic seismograms for a layered half-space with sources and receivers at close or same depth, *Pure Appl. Geophys.,* **160,** 467–486.

Zhang, W.B., Iwata, T., Irikura, K., Pitarka, A. & Sekiguchi, H., 2004. Dynamic rupture process of the 1999 Chi-Chi, Taiwan, earthquake, *Geophys. Res. Lett.,* **31,** L10605, doi:10.1029/2004GL109827.

APPENDIX A: PARTIAL DERIVATIVES OF GREEN'S FUNCTION WITH RESPECT TO x_3 OR/AND ξ_3

$$\tilde{\mathcal{G}}_{11}^{(i-1)}(\boldsymbol{x},\boldsymbol{\xi},\omega)=\frac{1}{4\pi\mu}\left\{\gamma_1^2\left[I_1^{(i)}+I_2^{(i)}\right]+\gamma_2^2\left[I_3^{(i)}+I_4^{(i)}\right]\right\}, \tag{A1.1}$$

$$\tilde{\mathcal{G}}_{12}^{(i-1)}(\boldsymbol{x},\boldsymbol{\xi},\omega)=\tilde{\mathcal{G}}_{21}^{(i-1)}(\boldsymbol{x},\boldsymbol{\xi},\omega)=\frac{1}{4\pi\mu}\gamma_1\gamma_2\left\{I_1^{(i)}+I_2^{(i)}-I_3^{(i)}-I_4^{(i)}\right\}, \tag{A1.2}$$

$$\tilde{\mathcal{G}}_{13}^{(i-1)}(\boldsymbol{x},\boldsymbol{\xi},\omega)=-\frac{1}{4\pi\mu}\gamma_1 I_5^{(i)}, \tag{A1.3}$$

$$\tilde{\mathcal{G}}_{22}^{(i-1)}(\boldsymbol{x},\boldsymbol{\xi},\omega)=\frac{1}{4\pi\mu}\left\{\gamma_2^2\left[I_1^{(i)}+I_2^{(i)}\right]+\gamma_1^2\left[I_3^{(i)}+I_4^{(i)}\right]\right\}, \tag{A1.4}$$

$$\tilde{\mathcal{G}}_{23}^{(i-1)}(\boldsymbol{x},\boldsymbol{\xi},\omega)=-\frac{1}{4\pi\mu}\gamma_2 I_5^{(i)}, \tag{A1.5}$$

$$\tilde{\mathcal{G}}_{31}^{(i-1)}(\boldsymbol{x},\boldsymbol{\xi},\omega)=-\frac{1}{4\pi\mu}\gamma_1 I_6^{(i)}, \tag{A1.6}$$

$$\tilde{\mathcal{G}}_{32}^{(i-1)}(\boldsymbol{x},\boldsymbol{\xi},\omega)=-\frac{1}{4\pi\mu}\gamma_2 I_6^{(i)}, \tag{A1.7}$$

$$\tilde{\mathcal{G}}_{33}^{(i-1)}(\boldsymbol{x},\boldsymbol{\xi},\omega)=-\frac{1}{4\pi\mu}I_7^{(i)}, \qquad (i=2,3,4,5) \tag{A1.8}$$

where

$$\tilde{\mathcal{G}}_{ij}^{(1)}=\tilde{G}_{ij,3}, \qquad \tilde{\mathcal{G}}_{ij}^{(2)}=\partial_3\tilde{G}_{ij}, \qquad \tilde{\mathcal{G}}_{ij}^{(3)}=\tilde{G}_{ij,33}, \qquad \tilde{\mathcal{G}}_{ij}^{(4)}=\partial_3\tilde{G}_{ij,3}, \tag{A2}$$

$$\begin{Bmatrix} I_1^{(i)} \\ I_3^{(i)} \end{Bmatrix}=\frac{1}{2}\int_0^{+\infty}A_{S1}^{(i)}(x_3,\xi_3,k,\omega)\left[J_0(kr)\mp J_2(kr)\right]dk, \tag{A3.1}$$

$$\begin{Bmatrix} I_2^{(i)} \\ I_4^{(i)} \end{Bmatrix}=\frac{1}{2}\int_0^{+\infty}A_{T}^{(i)}(x_3,\xi_3,k,\omega)\left[J_0(kr)\pm J_2(kr)\right]dk, \tag{A3.2}$$

$$I_5^{(i)}=\int_0^{+\infty}A_{S0}^{(i)}(x_3,\xi_3,k,\omega)J_1(kr)\,dk, \tag{A3.3}$$

$$I_6^{(i)}=\int_0^{+\infty}A_{R1}^{(i)}(x_3,\xi_3,k,\omega)J_1(kr)\,dk, \tag{A3.4}$$

$$I_7^{(i)}=\int_0^{+\infty}A_{R0}^{(i)}(x_3,\xi_3,k,\omega)J_0(kr)\,dk, \qquad (i=2,3,4,5) \tag{A3.5}$$

and

$$\begin{aligned}A_{S1}^{(2)}(x_3,\xi_3,k,\omega)=\frac{k\beta^2}{\omega^2}\Bigg\{&\mathrm{sgn}(x_3-\xi_3)(k^2e^{\mathrm{P}}-\nu^2e^{\mathrm{S}})+\frac{\bar{\mathcal{R}}(k)}{\mathcal{R}(k)}(k^2e^{\mathrm{PP}}+\nu^2e^{\mathrm{SS}})\\&-\frac{4k^2\nu\chi}{\mathcal{R}(k)}(\nu e^{\mathrm{SP}}+\gamma e^{\mathrm{PS}})\Bigg\},\end{aligned} \tag{A4.1}$$

$$A_{S0}^{(2)}(x_3,\xi_3,k,\omega)=\frac{k^2\beta^2}{\omega^2}\left\{(\gamma e^{\mathrm{P}}-\nu e^{\mathrm{S}})-\frac{\bar{\mathcal{R}}(k)}{\mathcal{R}(k)}(\gamma e^{\mathrm{PP}}+\nu e^{\mathrm{SS}})+\frac{4\nu\chi}{\mathcal{R}(k)}(k^2e^{\mathrm{SP}}+\gamma^2e^{\mathrm{PS}})\right\}, \tag{A4.2}$$

$$A_{R1}^{(2)}(x_3,\xi_3,k,\omega)=\frac{k^2\beta^2}{\omega^2}\left\{(\gamma e^{\mathrm{P}}-\nu e^{\mathrm{S}})+\frac{\bar{\mathcal{R}}(k)}{\mathcal{R}(k)}(\gamma e^{\mathrm{PP}}+\nu e^{\mathrm{SS}})-\frac{4\gamma\chi}{\mathcal{R}(k)}(\nu^2e^{\mathrm{SP}}+k^2e^{\mathrm{PS}})\right\}, \tag{A4.3}$$

$$A^{(2)}_{R0}(x_3,\xi_3,k,\omega)=\frac{k\beta^2}{\omega^2}\Big\{\mathrm{sgn}(x_3-\xi_3)(\gamma^2e^{\mathrm{P}}-k^2e^{\mathrm{S}})-\frac{\bar{\mathcal{R}}(k)}{\mathcal{R}(k)}(\gamma^2e^{\mathrm{PP}}+k^2e^{\mathrm{SS}})$$
$$+\frac{4k^2\gamma\chi}{\mathcal{R}(k)}(\nu e^{\mathrm{SP}}+\gamma e^{\mathrm{PS}})\Big\}, \tag{A4.4}$$

$$A^{(2)}_{T}(x_3,\xi_3,k,\omega)=k\Big\{\mathrm{sgn}(x_3-\xi_3)e^{\mathrm{S}}-e^{\mathrm{SS}}\Big\}, \tag{A4.5}$$

$$A^{(3)}_{S1}(x_3,\xi_3,k,\omega)=\frac{k\beta^2}{\omega^2}\Big\{-\mathrm{sgn}(x_3-\xi_3)(k^2e^{\mathrm{P}}-\nu^2e^{\mathrm{S}})+\frac{\bar{\mathcal{R}}(k)}{\mathcal{R}(k)}(k^2e^{\mathrm{PP}}+\nu^2e^{\mathrm{SS}})$$
$$-\frac{4k^2\nu\chi}{\mathcal{R}(k)}(\gamma e^{\mathrm{SP}}+\nu e^{\mathrm{PS}})\Big\}, \tag{A5.1}$$

$$A^{(3)}_{S0}(x_3,\xi_3,k,\omega)=\frac{k^2\beta^2}{\omega^2}\Big\{-(\gamma e^{\mathrm{P}}-\nu e^{\mathrm{S}})-\frac{\bar{\mathcal{R}}(k)}{\mathcal{R}(k)}(\gamma e^{\mathrm{PP}}+\nu e^{\mathrm{SS}})+\frac{4\gamma\chi}{\mathcal{R}(k)}(k^2e^{\mathrm{SP}}+\nu^2e^{\mathrm{PS}})\Big\}, \tag{A5.2}$$

$$A^{(3)}_{R1}(x_3,\xi_3,k,\omega)=\frac{k^2\beta^2}{\omega^2}\Big\{-(\gamma e^{\mathrm{P}}-\nu e^{\mathrm{S}})+\frac{\bar{\mathcal{R}}(k)}{\mathcal{R}(k)}(\gamma e^{\mathrm{PP}}+\nu e^{\mathrm{SS}})-\frac{4\nu\chi}{\mathcal{R}(k)}(\gamma^2e^{\mathrm{SP}}+k^2e^{\mathrm{PS}})\Big\}, \tag{A5.3}$$

$$A^{(3)}_{R0}(x_3,\xi_3,k,\omega)=\frac{k\beta^2}{\omega^2}\Big\{-\mathrm{sgn}(x_3-\xi_3)(\gamma^2e^{\mathrm{P}}-k^2e^{\mathrm{S}})-\frac{\bar{\mathcal{R}}(k)}{\mathcal{R}(k)}(\gamma^2e^{\mathrm{PP}}+k^2e^{\mathrm{SS}})$$
$$+\frac{4k^2\gamma\chi}{\mathcal{R}(k)}(\gamma e^{\mathrm{SP}}+\nu e^{\mathrm{PS}})\Big\}, \tag{A5.4}$$

$$A^{(3)}_{T}(x_3,\xi_3,k,\omega)=-k\Big\{\mathrm{sgn}(x_3-\xi_3)e^{\mathrm{S}}+e^{\mathrm{SS}}\Big\}, \tag{A5.5}$$

$$A^{(4)}_{S1}(x_3,\xi_3,k,\omega)=\frac{k\beta^2}{\omega^2}\Big\{(k^2\gamma e^{\mathrm{P}}-\nu^3e^{\mathrm{S}})-\frac{\bar{\mathcal{R}}(k)}{\mathcal{R}(k)}(k^2\gamma e^{\mathrm{PP}}+\nu^3e^{\mathrm{SS}})+\frac{4k^2\nu\chi}{\mathcal{R}(k)}(\nu^2e^{\mathrm{SP}}+\gamma^2e^{\mathrm{PS}})\Big\}, \tag{A6.1}$$

$$A^{(4)}_{S0}(x_3,\xi_3,k,\omega)=\frac{k^2\beta^2}{\omega^2}\Big\{\mathrm{sgn}(x_3-\xi_3)(\gamma^2e^{\mathrm{P}}-\nu^2e^{\mathrm{S}})+\frac{\bar{\mathcal{R}}(k)}{\mathcal{R}(k)}(\gamma^2e^{\mathrm{PP}}+\nu^2e^{\mathrm{SS}})$$
$$-\frac{4\nu\chi}{\mathcal{R}(k)}(k^2\nu e^{\mathrm{SP}}+\gamma^3e^{\mathrm{PS}})\Big\}, \tag{A6.2}$$

$$A^{(4)}_{R1}(x_3,\xi_3,k,\omega)=\frac{k^2\beta^2}{\omega^2}\Big\{\mathrm{sgn}(x_3-\xi_3)(\gamma^2e^{\mathrm{P}}-\nu^2e^{\mathrm{S}})-\frac{\bar{\mathcal{R}}(k)}{\mathcal{R}(k)}(\gamma^2e^{\mathrm{PP}}+\nu^2e^{\mathrm{SS}})$$
$$+\frac{4\gamma\chi}{\mathcal{R}(k)}(\nu^3e^{\mathrm{SP}}+k^2\gamma e^{\mathrm{PS}})\Big\}, \tag{A6.3}$$

$$A^{(4)}_{R0}(x_3,\xi_3,k,\omega)=\frac{k\beta^2}{\omega^2}\Big\{(\gamma^3e^{\mathrm{P}}-k^2\nu e^{\mathrm{S}})+\frac{\bar{\mathcal{R}}(k)}{\mathcal{R}(k)}(\gamma^3e^{\mathrm{PP}}+k^2\nu e^{\mathrm{SS}})-\frac{4k^2\gamma\chi}{\mathcal{R}(k)}(\nu^2e^{\mathrm{SP}}+\gamma^2e^{\mathrm{PS}})\Big\}, \tag{A6.4}$$

$$A^{(4)}_{T}(x_3,\xi_3,k,\omega)=k\nu\Big\{e^{\mathrm{S}}+e^{\mathrm{SS}}\Big\}, \tag{A6.5}$$

$$A^{(5)}_{S1}(x_3,\xi_3,k,\omega)=\frac{k\beta^2}{\omega^2}\Big\{-(k^2\gamma e^{\mathrm{P}}-\nu^3e^{\mathrm{S}})-\frac{\bar{\mathcal{R}}(k)}{\mathcal{R}(k)}(k^2\gamma e^{\mathrm{PP}}+\nu^3e^{\mathrm{SS}})+\frac{4k^2\nu^2\gamma\chi}{\mathcal{R}(k)}(e^{\mathrm{SP}}+e^{\mathrm{PS}})\Big\}, \tag{A7.1}$$

$$A^{(5)}_{S0}(x_3,\xi_3,k,\omega)=\frac{k^2\beta^2}{\omega^2}\Big\{-\mathrm{sgn}(x_3-\xi_3)(\gamma^2e^{\mathrm{P}}-\nu^2e^{\mathrm{S}})+\frac{\bar{\mathcal{R}}(k)}{\mathcal{R}(k)}(\gamma^2e^{\mathrm{PP}}+\nu^2e^{\mathrm{SS}})$$
$$-\frac{4\nu\gamma\chi}{\mathcal{R}(k)}(k^2e^{\mathrm{SP}}+\nu\gamma e^{\mathrm{PS}})\Big\}, \tag{A7.2}$$

$$A^{(5)}_{R1}(x_3,\xi_3,k,\omega)=\frac{k^2\beta^2}{\omega^2}\Big\{-\mathrm{sgn}(x_3-\xi_3)(\gamma^2e^{\mathrm{P}}-\nu^2e^{\mathrm{S}})-\frac{\bar{\mathcal{R}}(k)}{\mathcal{R}(k)}(\gamma^2e^{\mathrm{PP}}+\nu^2e^{\mathrm{SS}})$$
$$+\frac{4\nu\gamma\chi}{\mathcal{R}(k)}(\nu\gamma e^{\mathrm{SP}}+k^2e^{\mathrm{PS}})\Big\}, \tag{A7.3}$$

$$A^{(5)}_{R0}(x_3,\xi_3,k,\omega)=\frac{k\beta^2}{\omega^2}\Big\{-(\gamma^3e^{\mathrm{P}}-k^2\nu e^{\mathrm{S}})+\frac{\bar{\mathcal{R}}(k)}{\mathcal{R}(k)}(\gamma^3e^{\mathrm{PP}}+k^2\nu e^{\mathrm{SS}})-\frac{4k^2\nu\gamma^2\chi}{\mathcal{R}(k)}(e^{\mathrm{SP}}+e^{\mathrm{PS}})\Big\}, \tag{A7.4}$$

$$A_T^{(5)}(x_3,\xi_3,k,\omega)=k\nu\Big\{-e^{\mathrm{S}}+e^{\mathrm{SS}}\Big\}. \tag{A7.5}$$

APPENDIX B: TAYLOR'S EXPANSIONS FOR $A_{\mathrm{S1}}^{\mathrm{asy(i)}}$, $A_{\mathrm{S0}}^{\mathrm{asy(i)}}$, $A_{\mathrm{R1}}^{\mathrm{asy(i)}}$, $A_{\mathrm{R0}}^{\mathrm{asy(i)}}$, $A_T^{\mathrm{asy(i)}}$ AND ANALYTIC SOLUTIONS OF Q_{mn}

Here are the full lists of $A_{S1}^{\mathrm{asy}(i)}$, $A_{S0}^{\mathrm{asy}(i)}$, $A_{R1}^{\mathrm{asy}(i)}$, $A_{R0}^{\mathrm{asy}(i)}$, $A_T^{\mathrm{asy}(i)}$ ($i=1,2,\ldots,5$) and Q_{mn} ($m=0,1,2;n=0,1,2,3$):

$$A_{S1}^{\mathrm{asy}(1)}(x_3,\xi_3,k,\omega)=-\Big[\frac{1-p}{2}\,|x_3-\xi_3|\,k^2+\frac{\omega^2}{8\beta^2}(1-p^2)(x_3-\xi_3)^2k-\frac{1+p}{2}k$$
$$-\frac{\omega^2}{8\beta^2}(1+3p^2)\,|x_3-\xi_3|+\frac{\omega^4}{48\beta^4}(1-p^3)\,|x_3-\xi_3|^3\Big]e^{-k|x_3-\xi_3|}, \tag{B1.1}$$

$$A_{S0}^{\mathrm{asy}(1)}(x_3,\xi_3,k,\omega)=-\mathrm{sgn}(x_3-\xi_3)\Big[\frac{1-p}{2}\,|x_3-\xi_3|\,k^2+\frac{\omega^2}{8\beta^2}(1-p^2)(x_3-\xi_3)^2k$$
$$+\frac{\omega^2}{8\beta^2}(1-p^2)\,|x_3-\xi_3|+\frac{\omega^4}{48\beta^4}(1-p^3)\,|x_3-\xi_3|^3\Big]e^{-k|x_3-\xi_3|}, \tag{B1.2}$$

$$A_{R1}^{\mathrm{asy}(1)}(x_3,\xi_3,k,\omega)=A_{S0}^{\mathrm{asy}(1)}(x_3,\xi_3,k,\omega), \tag{B1.3}$$

$$A_{R0}^{\mathrm{asy}(1)}(x_3,\xi_3,k,\omega)=-\Big[\frac{1-p}{2}\,|x_3-\xi_3|\,k^2+\frac{\omega^2}{8\beta^2}(1-p^2)(x_3-\xi_3)^2k+\frac{1+p}{2}k$$
$$+\frac{\omega^2}{8\beta^2}(3+p^2)\,|x_3-\xi_3|+\frac{\omega^4}{48\beta^4}(1-p^3)\,|x_3-\xi_3|^3\Big]e^{-k|x_3-\xi_3|}, \tag{B1.4}$$

$$A_T^{\mathrm{asy}(1)}(x_3,\xi_3,k,\omega)=\Big[k+\frac{\omega^2}{2\beta^2}\,|x_3-\xi_3|\Big]e^{-k|x_3-\xi_3|}, \tag{B1.5}$$

$$A_{S1}^{\mathrm{asy}(2)}(x_3,\xi_3,k,\omega)=-A_{S1}^{\mathrm{asy}(3)}(x_3,\xi_3,k,\omega)=-\mathrm{sgn}(x_3-\xi_3)\Big[\frac{1-p}{2}\,|x_3-\xi_3|\,k^2+\frac{\omega^2}{8\beta^2}(1-p^2)$$
$$\times(x_3-\xi_3)^2k-k-\frac{\omega^2}{8\beta^2}(3+p^2)\,|x_3-\xi_3|+\frac{\omega^4}{48\beta^4}(1-p^3)\,|x_3-\xi_3|^3\Big]e^{-k|x_3-\xi_3|}, \tag{B1.6}$$

$$A_{S0}^{\mathrm{asy}(2)}(x_3,\xi_3,k,\omega)=-A_{S0}^{\mathrm{asy}(3)}(x_3,\xi_3,k,\omega)=-\Big[\frac{1-p}{2}\,|x_3-\xi_3|\,k^2+\frac{\omega^2}{8\beta^2}(1-p^2)(x_3-\xi_3)^2k$$
$$-\frac{1-p}{2}k-\frac{\omega^2}{8\beta^2}(1-p^2)\,|x_3-\xi_3|+\frac{\omega^4}{48\beta^4}(1-p^3)\,|x_3-\xi_3|^3\Big]e^{-k|x_3-\xi_3|}, \tag{B1.7}$$

$$A_{R1}^{\mathrm{asy}(2)}(x_3,\xi_3,k,\omega)=-A_{R1}^{\mathrm{asy}(3)}(x_3,\xi_3,k,\omega)=A_{S0}^{\mathrm{asy}(2)}(x_3,\xi_3,k,\omega), \tag{B1.8}$$

$$A_{R0}^{\mathrm{asy}(2)}(x_3,\xi_3,k,\omega)=-A_{R0}^{\mathrm{asy}(3)}(x_3,\xi_3,k,\omega)=-\mathrm{sgn}(x_3-\xi_3)\Big[\frac{1-p}{2}\,|x_3-\xi_3|\,k^2+\frac{\omega^2}{8\beta^2}(1-p^2)$$
$$\times(x_3-\xi_3)^2k+pk+\frac{\omega^2}{8\beta^2}(1+3p^2)\,|x_3-\xi_3|+\frac{\omega^4}{48\beta^4}(1-p^3)\,|x_3-\xi_3|^3\Big]e^{-k|x_3-\xi_3|}, \tag{B1.9}$$

$$A_T^{\mathrm{asy}(2)}(x_3,\xi_3,k,\omega)=-A_T^{\mathrm{asy}(3)}(x_3,\xi_3,k,\omega)=\mathrm{sgn}(x_3-\xi_3)\Big[k+\frac{\omega^2}{2\beta^2}\,|x_3-\xi_3|\Big]e^{-k|x_3-\xi_3|}, \tag{B1.10}$$

$$A_{S1}^{\mathrm{asy}(4)}(x_3,\xi_3,k,\omega)=-A_{S1}^{\mathrm{asy}(5)}(x_3,\xi_3,k,\omega)=-\Big[\frac{1-p}{2}\,|x_3-\xi_3|\,k^3+\frac{\omega^2}{8\beta^2}(1-p^2)(x_3-\xi_3)^2k^2$$
$$-\frac{3-p}{2}k^2-\frac{\omega^2}{8\beta^2}(5-p^2)\,|x_3-\xi_3|\,k+\frac{\omega^4}{48\beta^4}(1-p^3)\,|x_3-\xi_3|^3\,k+\frac{\omega^2}{8\beta^2}(3+p^2)$$
$$-\frac{\omega^4}{8\beta^4}(x_3-\xi_3)^2+\frac{\omega^6}{384\beta^6}(1-p^4)(x_3-\xi_3)^4\Big]e^{-k|x_3-\xi_3|}, \tag{B1.11}$$

$$A_{S0}^{\mathrm{asy}(4)}(x_3,\xi_3,k,\omega)=-A_{S0}^{\mathrm{asy}(5)}(x_3,\xi_3,k,\omega)=-\mathrm{sgn}(x_3-\xi_3)\Big[\frac{1-p}{2}\,|x_3-\xi_3|\,k^3+\frac{\omega^2}{8\beta^2}(1-p^2)$$
$$\times(x_3-\xi_3)^2k^2-(1-p)k^2-\frac{3\omega^2}{8\beta^2}(1-p^2)\,|x_3-\xi_3|\,k+\frac{\omega^4}{48\beta^4}(1-p^3)\,|x_3-\xi_3|^3\,k$$
$$-\frac{\omega^4}{16\beta^4}(1-p^3)(x_3-\xi_3)^2+\frac{\omega^6}{384\beta^6}(1-p^4)(x_3-\xi_3)^4\Big]e^{-k|x_3-\xi_3|}, \tag{B1.12}$$

$$A_{R1}^{\mathrm{asy}(4)}(x_3,\xi_3,k,\omega) = -A_{R1}^{\mathrm{asy}(5)}(x_3,\xi_3,k,\omega) = A_{S0}^{\mathrm{asy}(4)}(x_3,\xi_3,k,\omega), \tag{B1.13}$$

$$\begin{aligned} A_{R0}^{\mathrm{asy}(4)}(x_3,\xi_3,k,\omega) = -A_{R0}^{\mathrm{asy}(5)}(x_3,\xi_3,k,\omega) = -\Bigg[& \frac{1-p}{2}\,|x_3-\xi_3|\,k^3 + \frac{\omega^2}{8\beta^2}(1-p^2)(x_3-\xi_3)^2k^2 \\ & -\frac{1-3p}{2}k^2 - \frac{\omega^2}{8\beta^2}(1-5p^2)\,|x_3-\xi_3|\,k + \frac{\omega^4}{48\beta^4}(1-p^3)\,|x_3-\xi_3|^3\,k - \frac{\omega^2}{8\beta^2}(1+3p^2) \\ & +\frac{\omega^4}{8\alpha^4}p\,(x_3-\xi_3)^2 + \frac{\omega^6}{384\beta^6}(1-p^4)\,(x_3-\xi_3)^4\Bigg] e^{-k|x_3-\xi_3|}, \end{aligned} \tag{B1.14}$$

$$\begin{aligned} A_{T}^{\mathrm{asy}(4)}(x_3,\xi_3,k,\omega) = -A_{T}^{\mathrm{asy}(5)}(x_3,\xi_3,k,\omega) = & \left[k^2 + \frac{\omega^2}{2\beta^2}\,|x_3-\xi_3|\,k - \frac{\omega^2}{2\beta^2} + \frac{\omega^4}{8\beta^4}\,(x_3-\xi_3)^2\right] \\ & \times e^{-k|x_3-\xi_3|}, \end{aligned} \tag{B1.15}$$

where $p = \dfrac{\mu}{\lambda+2\mu}$, λ and μ being the Lamé's constants and

$$\begin{aligned} &Q_{00}(r,x_3-\xi_3) = \tfrac{1}{R}, && Q_{01}(r,x_3-\xi_3) = \tfrac{|x_3-\xi_3|}{R^3}, \\ &Q_{02}(r,x_3-\xi_3) = \tfrac{2(x_3-\xi_3)^2-r^2}{R^5}, && Q_{03}(r,x_3-\xi_3) = \tfrac{3|x_3-\xi_3|\left[2(x_3-\xi_3)^2-3r^2\right]}{R^7}, \\ &Q_{10}(r,x_3-\xi_3) = \tfrac{R-|x_3-\xi_3|}{rR}, && Q_{11}(r,x_3-\xi_3) = \tfrac{r}{R^3}, \\ &Q_{12}(r,x_3-\xi_3) = \tfrac{3r|x_3-\xi_3|}{R^5}, && Q_{13}(r,x_3-\xi_3) = \tfrac{3r\left[4(x_3-\xi_3)^2-r^2\right]}{R^7}, \\ &Q_{20}(r,x_3-\xi_3) = \tfrac{(R-|x_3-\xi_3|)^2}{r^2R}, && Q_{21}(r,x_3-\xi_3) = \tfrac{2}{r}Q_{10}(r,x_3-\xi_3) - Q_{01}(r,x_3-\xi_3), \\ &Q_{22}(r,x_3-\xi_3) = \tfrac{3r^2}{R^5}, && Q_{23}(r,x_3-\xi_3) = \tfrac{15r^2|x_3-\xi_3|}{R^7}. \end{aligned} \tag{B2}$$